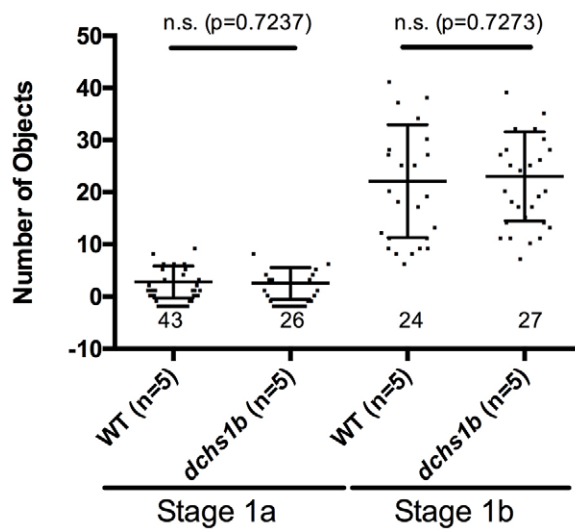


CORRECTION

Dachsous1b cadherin regulates actin and microtubule cytoskeleton during early zebrafish embryogenesis

Nanbing Li-Villarreal, Meredyth M. Forbes, Andrew J. Loza, Jiakun Chen, Taylur Ma, Kathryn Hede, Cecilia B. Moens, Jimann Shin, Atsushi Sawada, Anna E. Hindes, Julien Dubrulle, Alexander F. Schier, Gregory D. Longmore, Florence L. Marlow and Lilianna Solnica-Krezel

In Development **142**, 2704-2718, the data presented in Figure 2F indicated that there was a significant reduction in acetylated microtubules in stage Ia and Ib *dachsous1b* oocytes compared with wild-type oocytes, but that *dachsous1b* and wild-type oocytes were comparable by stage II of oogenesis. Based on these data and other oocyte analyses reported in the paper, we concluded that *dachsous1b* oogenesis is largely unaffected. The second author (M.M.F.) admitted that, without the knowledge of the other authors, she manipulated the stage Ia and stage Ib mutant data shown in the original Figure 2F. Therefore, we repeated this experiment and examined five wild-type and five *dachsous* mutant ovaries (>20 oocytes per genotype per stage), and found no significant differences in acetylated microtubules between wild-type and *dachsous* mutant oocytes at any of the stages examined. These new data, which are presented in the corrected figure (below), further support the overall conclusion reported in the original paper that oogenesis is intact in *dachsous1b* mutants. As the major conclusions of the paper are not affected, the journal editors – following consultation with all authors and the Academic Affairs Committee at Albert Einstein College of Medicine – have agreed that a Correction should be provided, with an explanation of the circumstances. This course of action complies with the journal's policy on correction of issues in the scientific record, which states: 'Should an error appear in a published article that affects scientific meaning or author credibility but does not affect the overall results and conclusions of the paper, our policy is to publish a Correction'. We regret any confusion this may have caused.



RESEARCH ARTICLE

Dachsous1b cadherin regulates actin and microtubule cytoskeleton during early zebrafish embryogenesis

Nanbing Li-Villarreal¹, Meredith M. Forbes², Andrew J. Loza³, Jiakun Chen¹, Taylor Ma⁴, Kathryn Hede⁴, Cecilia B. Moens⁴, Jimann Shin¹, Atsushi Sawada¹, Anna E. Hindes¹, Julien Dubrulle⁵, Alexander F. Schier⁵, Gregory D. Longmore³, Florence L. Marlow^{2,6} and Lilianna Solnica-Krezel^{1,*}

ABSTRACT

Dachsous (Dchs), an atypical cadherin, is an evolutionarily conserved regulator of planar cell polarity, tissue size and cell adhesion. In humans, *DCHS1* mutations cause pleiotropic Van Maldergem syndrome. Here, we report that mutations in zebrafish *dchs1b* and *dchs2* disrupt several aspects of embryogenesis, including gastrulation. Unexpectedly, maternal zygotic (MZ) *dchs1b* mutants show defects in the earliest developmental stage, egg activation, including abnormal cortical granule exocytosis (CGE), cytoplasmic segregation, cleavages and maternal mRNA translocation, in transcriptionally quiescent embryos. Later, MZ *dchs1b* mutants exhibit altered dorsal organizer and mesendodermal gene expression, due to impaired dorsal determinant transport and Nodal signaling. Mechanistically, MZ *dchs1b* phenotypes can be explained in part by defective actin or microtubule networks, which appear bundled in mutants. Accordingly, disruption of actin cytoskeleton in wild-type embryos phenocopied MZ *dchs1b* mutant defects in cytoplasmic segregation and CGE, whereas interfering with microtubules in wild-type embryos impaired dorsal organizer and mesodermal gene expression without perceptible earlier phenotypes. Moreover, the bundled microtubule phenotype was partially rescued by expressing either full-length Dchs1b or its intracellular domain, suggesting that Dchs1b affects microtubules and some developmental processes independent of its known ligand Fat. Our results indicate novel roles for vertebrate Dchs in actin and microtubule cytoskeleton regulation in the unanticipated context of the single-celled embryo.

KEY WORDS: Actin, Cell fate, *dchs1b*, Egg activation, Microtubule, Morphogenesis

INTRODUCTION

Dachsous is an evolutionarily conserved large cadherin, with roles in vertebrate embryogenesis that are only beginning to be understood. Dachsous features 27 extracellular cadherin repeats, a single-pass transmembrane and an intracellular domain (Clark et al., 1995). In *Drosophila*, where *dachsous* was first identified, it functions in tissue growth control upstream of Hippo signaling

(Clark et al., 1995) and planar cell polarity (PCP), the process of polarizing cells within the tissue plane, acting in part through an unconventional myosin, Dachs (Cho and Irvine, 2004; Mao et al., 2006). Studies in *Drosophila* and cell culture demonstrated that Dachsous mediates PCP and cell adhesion via heterophilic intercellular interactions with another cadherin, Fat (Ishiiuchi et al., 2009; Matakatsu and Blair, 2004; Takeichi, 1995). In *Drosophila*, phosphorylation of cadherin repeats by the Golgi-localized kinase Four-jointed modulates these interactions (Ishikawa et al., 2008; Simon et al., 2010). Non-mutually exclusive models for Dachsous function in planar polarity posit that it acts upstream and/or parallel to the core PCP components (Adler et al., 1998; Casal et al., 2006, 2002; Donoughe and DiNardo, 2011; Ma et al., 2003; Matis et al., 2014; Rawls et al., 2002; Yang et al., 2002).

Less is known about the two vertebrate homologs, *Dachsous1* (*Dchs1*) and *Dachsous2* (*Dchs2*). Mice homozygous for an N-terminal deletion of *Dchs1* die postnatally, exhibiting abnormalities in multiple organs (Mao et al., 2011) and defects in migration of hindbrain branchiomotor neurons (Zakaria et al., 2014). Mutations in human *DCHS1* were recently linked to recessive Van Maldergem syndrome, with pleiotropic phenotypes including neuronal periventricular heterotopia (Cappello et al., 2013). These data establish a requirement for *Dchs1* during vertebrate organogenesis, but the underlying cellular mechanisms are unknown.

Here, we examine Dchs roles in vertebrate development using zebrafish, the genome of which contains three *dchs* genes, *dchs1a*, *dchs1b* and *dchs2*, with *dchs1a* and *dchs1b* probably resulting from genome duplication (Taylor et al., 2003). Through mutational analyses, we uncovered essential overlapping and unique roles for *dchs1b* and *dchs2* during embryogenesis. Unexpectedly, maternal *dchs1b* activity is uniquely required for egg activation, focusing our investigation on early *dchs1b* developmental functions.

Vertebrate embryogenesis is initiated by egg activation and fertilization, followed by cell cleavages generating the blastula, which then gastrulates to form the germ layers and basic body plan (Solnica-Krezel, 2005; Stern, 1992). Zebrafish eggs, composed of intermixed cytoplasm and yolk, exhibit animal-vegetal polarity (Houston, 2013; Wallace and Selman, 1990). Egg activation triggers cortical granule exocytosis (CGE) and cytoplasmic streaming to form the blastodisc at the animal pole. Cortical granules (CG) release their contents at the egg cortex, contributing to chorion expansion and surface remodeling (Fuentes and Fernandez, 2010; Hart, 1990; Tsaadon et al., 2006; Wong and Wessel, 2006). Stabilizing or destabilizing F-actin established the dependence of both CGE and cytoplasmic streaming on a dynamic actin cytoskeleton (Becker and Hart, 1999; Fernandez et al., 2006; Hart and Fluck, 1996; Ivanenkov et al., 1987; Leung et al., 2000; Wolenski and Hart, 1988). Maternally deposited dorsal

¹Department of Developmental Biology, Washington University School of Medicine in St. Louis, St. Louis, MO 63110, USA. ²Department of Developmental and Molecular Biology, Albert Einstein College of Medicine, Yeshiva University, Bronx, NY 10461, USA. ³Department of Internal Medicine, Washington University School of Medicine in St. Louis, St. Louis, MO 63110, USA. ⁴Division of Basic Sciences, Fred Hutchinson Cancer Research Center, Seattle, WA 98109, USA. ⁵Department of Molecular and Cellular Biology, Harvard University, Cambridge, MA 02138, USA. ⁶Department of Neuroscience, Albert Einstein College of Medicine, Yeshiva University, Bronx, NY 10461, USA.

*Author for correspondence (solnical@wustl.edu)

Received 12 November 2014; Accepted 25 June 2015

determinants (DDs), including *wnt8a* mRNA, reside at the vegetal pole (Kosaka et al., 2007; Lu et al., 2011). Embryonic patterning requires these vegetally located molecules, as their removal, either surgically (Jesuthasan and Strähle, 1997; Mizuno et al., 1999) or by maternal-effect mutations, impairs dorsal axis specification (Ge et al., 2014; Nojima et al., 2010). During early cleavages, a dynamic vegetal microtubule network mediates asymmetric transport of DDs (Lu et al., 2011; Nojima et al., 2004; Tran et al., 2012), which accumulate in a few marginal blastomeres to establish the Nieuwkoop center, a key regulator of axis determination (Gore and Sampath, 2002; Jesuthasan and Strähle, 1997; Lu et al., 2011). Disruption of these microtubule arrays impairs DD transport and axis formation (Ge et al., 2014; Gore and Sampath, 2002; Jesuthasan and Strähle, 1997; Lu et al., 2011; Nojima et al., 2004; Tran et al., 2012).

Midblastula transition (MBT) occurs around the tenth cell division, when marginal blastomeres collapse into the yolk, forming the yolk syncytial layer (YSL), zygotic transcription starts and cell divisions become asynchronous (Kane and Kimmel, 1993; Kimmel et al., 1995). The YSL is crucial for embryonic patterning and morphogenesis (Carvalho and Heisenberg, 2010; Fekany et al., 1999; Mizuno et al., 1999). Dorsal YSL and marginal blastomeres constitute the Nieuwkoop center where DDs promote nuclear accumulation of maternal β -catenin, which activates zygotic transcriptional regulators, including Bozozok/Dharma and secreted Nodal morphogens, to induce the gastrula organizer and specify mesendoderm (Carvalho and Heisenberg, 2010; Lachnit et al., 2008; Mizuno et al., 1999; Rodaway et al., 1999; Shimizu et al., 2000; Sirotnik et al., 2000; Solnica-Krezel and Driever, 2001).

We generated zebrafish maternal (MZ) *dchs1b* and MZ*dchs2* mutants and found that they exhibit epiboly and convergence and extension (C&E) defects during gastrulation, whereas only MZ*dchs1b* mutants display egg activation and cell fate specification defects. Signifying that MZ*dchs1b* phenotypes are due to cytoskeletal abnormalities, actin and microtubule networks in MZ*dchs1b* mutants appeared excessively bundled, defects that were partially rescued by expressing either full-length or Dchs1b intracellular domain. Accordingly, pharmacologic interference with actin or microtubule dynamics in wild-type (WT) embryos phenocopied mutant defects in egg activation or dorsal mesoderm specification, respectively. Together, these results uncover novel roles for Dchs1b in embryonic patterning and morphogenesis through regulation of actin and microtubules, probably independent of its intercellular ligand Fat.

RESULTS

Generation of nonsense mutations in zebrafish *dchs1b* and *dchs2* genes

Quantitative RT-PCR (qRT-PCR) revealed that zebrafish *dchs1a*, *dchs1b* and *dchs2* genes were expressed maternally and zygotically (Fig. 1A). Notably, *dchs1b* transcripts were more abundant maternally, whereas expression of both *dchs1a* and *dchs2* peaked during zygotic stages (Fig. 1A). Whole-mount *in situ* hybridization (WISH) of *dchs* transcripts revealed similar ubiquitous distribution during embryogenesis and enrichment in neural tissues at 24 hpf (Fig. 1B; supplementary material Fig. S1A). To investigate the unique and overlapping functions of the three *dchs* genes we generated two nonsense mutations in *dchs1b* and one nonsense mutation in *dchs2* through ‘Targeting Induced Local Lesions IN Genomes’ (TILLING) (Draper et al., 2004; Wienholds and Plasterk, 2004). *dchs1b*^{h274} (C11527T; Q924) and *dchs1b*^{h275} (C11683T; Q976) mutations both generated amber stop codons, whereas *dchs2*^{stl1} (T6528A; Y201)

mutation yielded the ochre stop codon, with all three mutations predicted to truncate the proteins early in the extracellular domains (Fig. 1C,D). qRT-PCR analysis revealed significant reduction of *dchs1b* and *dchs2* mRNA levels in both alleles of MZ*dchs1b* and MZ*dchs2* mutants, respectively, compared with WT (Fig. 1E; supplementary material Fig. S1B). Notably, *dchs1a* and *dchs2* transcript abundance in MZ*dchs1b* mutants and *dchs1a* and *dchs1b* transcript in MZ*dchs2* mutants were unchanged (supplementary material Fig. S1C-E). These results are consistent with nonsense-mediated degradation of mRNA encoded by all mutant alleles (Chang et al., 2007), indicating null or severe hypomorphic mutations.

MZ*dchs1b* mutants display pleiotropic defects during embryogenesis

Zygotic *dchs1b* and *dchs2* mutants showed no overt developmental anomalies and developed into fertile adults. Morphological analysis of *in vitro*-fertilized time-matched progeny of WT and *dchs1b* or *dchs2* mutant parents revealed an overall developmental delay of MZ mutants (Fig. 1F). MZ mutants required 5.5 h, compared with 4 h for WT, to progress from the shield to yolk plug closure stage, indicating slower epiboly. Examination of the relative positions of cell type-specific markers to diagnose C&E movements in stage-matched mutant and WT gastrulae (Jessen et al., 2002) revealed a mediolaterally wider and anteroposteriorly shorter notochord marked by *no tail/brachury* (*ntl*) expression in mutant gastrulae at 70% epiboly (Schulte-Merker et al., 1992), suggesting defective C&E movements (Fig. 1G,H). At early segmentation, the *hgg1*-expressing prechordal plate was positioned anterior to the arc-shaped *dlx3* domain demarcating neuroectoderm. However, in mutants, the *hgg1* domain overlapped with or was positioned posterior to the *dlx3* domain, which was also mediolaterally wider, typical of impaired prechordal mesoderm migration or C&E movements (Heisenberg et al., 2000; Marlow et al., 1998; Topczewski et al., 2001) (Fig. 1I,J).

Next, we investigated whether delayed gastrulation was due to earlier defects. Whereas MZ*dchs2*^{stl1/stl1} mutants progressed through cleavage and blastula stages normally, compared with time-matched WT embryos, MZ*dchs1b*^{h275/h275} mutants displayed defects beginning from fertilization, including smaller blastodiscs with non-uniform cleavages, thus producing variably sized blastomeres (Fig. 1F and Fig. 4C). We detected globular yolk-like inclusions in the blastodiscs of MZ*dchs1b*^{h275/h275}, hereafter called MZ*dchs1b* mutants, but not in WT blastodiscs (Fig. 1F). These defects varied in penetrance and expressivity, with the most severe resulting in lethality by 24 hpf. Typically, fewer than 30% of mutants survived beyond 24 hpf compared with 80% of WT embryos (supplementary material Fig. S2A). Images in Fig. 1F represent moderate mutant phenotypes. MZ*dchs1b*^{h274/h274} mutants showed a similar array of abnormalities, indicating that these defects are specific to loss of maternal and zygotic *dchs1b* function (supplementary material Fig. S2D). MZ*dchs1b*^{h275/h275}; MZ*dchs2*^{stl1/stl1} compound mutant phenotypes resembled those of single MZ*dchs1b* embryos, albeit occurring with higher penetrance and more uniform expressivity (Fig. 1F and Fig. 5A,E,G; data not shown). Detailed analyses of *dchs* functions during gastrulation will be described elsewhere. Hereafter, we further investigate the early developmental roles of MZ*dchs1b*.

Largely normal progression of oogenesis in MZ*dchs1b* mutants

As defects were already apparent in MZ*dchs* eggs upon fertilization, we investigated potential *dchs* roles in oogenesis. Zebrafish oogenesis consists of five stages with characteristic features that

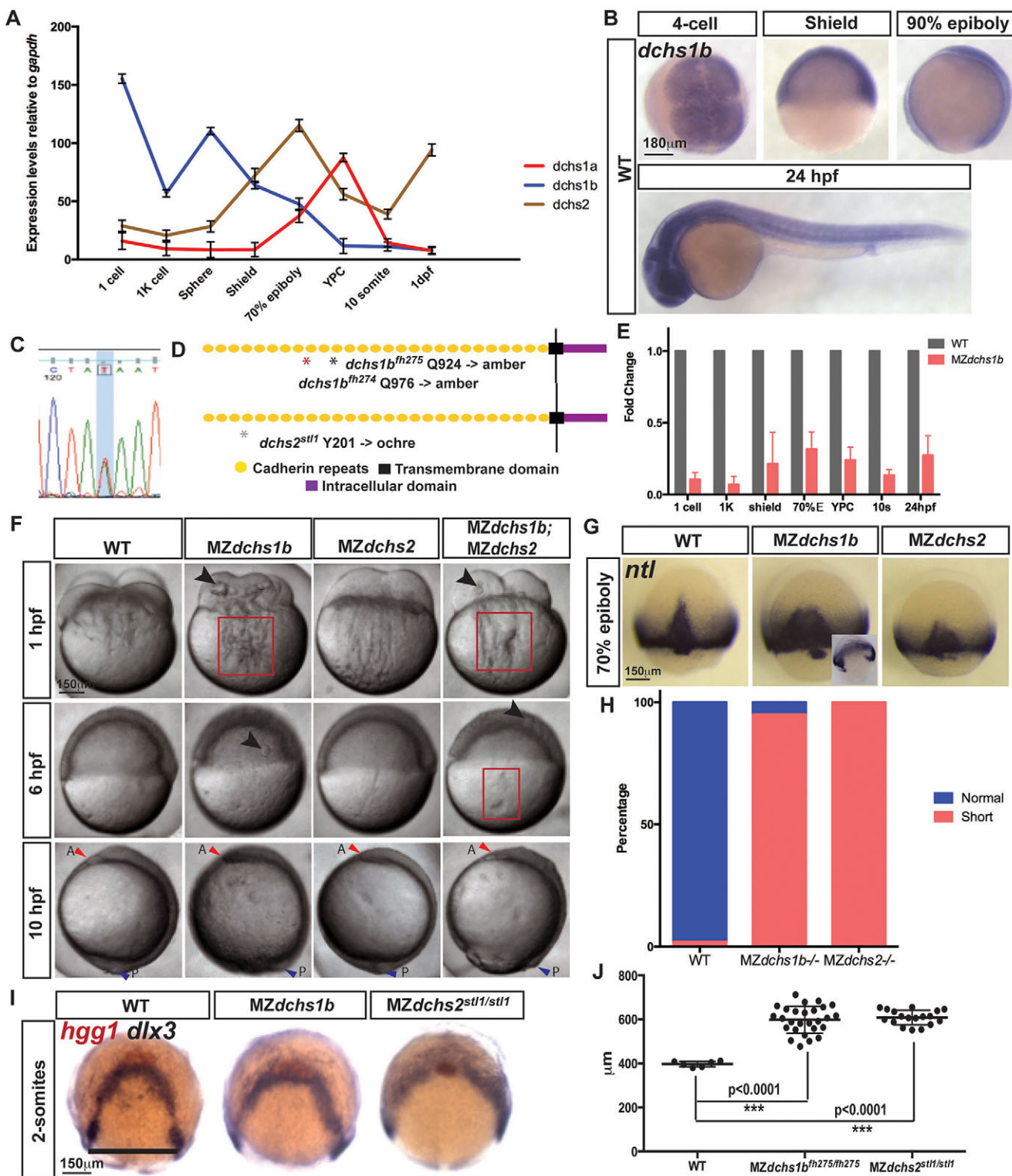


Fig. 1. Spatiotemporal expression and mutations in zebrafish *dchs* genes leading to pleiotropic defects during embryogenesis. (A) qRT-PCR analysis of the expression of all three zebrafish *dchs* genes at maternal and zygotic stages normalized to *gapdh* transcripts. (B) Whole-mount *in situ* hybridization (WISH) of *dchs1b* in WT embryos at four-cell, shield, 90% epiboly and 24-hpf stages. (C) Sanger sequencing trace for *dchs2* A-to-T mutations. (D) Schematic of Dchs protein, with mutations denoted by asterisks. (E) qRT-PCR analysis of *dchs1b* expression in MZdchs1b relative to WT embryos at maternal and zygotic stages. (F) Bright-field images of WT, MZdchs1b, MZdchs2^{s_{st1}/s_{st1}} and MZdchs1b^{f_{h275/f_{h275}}};MZdchs2^{s_{st1}/s_{st1}} time-matched embryos at 1, 6 and 10 hpf. Red boxes indicate distortions in the yolk cell. Large arrowheads denote yolk masses in the blastoderm. Small red arrowheads indicate anterior (A); small blue arrowheads indicate posterior (P). (G) *ntl* WISH for stage-matched WT, MZdchs1b and MZdchs2^{s_{st1}/s_{st1}} embryos at 70% epiboly. Inset depicts time-matched MZdchs1b embryo with a gap in the *ntl* expression domain. (H) Quantification of axial mesoderm length in WT ($n=111$), MZdchs1b ($n=414$) and MZdchs2^{s_{st1}/s_{st1}} ($n=486$) embryos. (I) *hgg1* and *dlx3* WISH analysis of WT, MZdchs1b and MZdchs2^{s_{st1}/s_{st1}} stage-matched embryos at two-somite stage (12 hpf). (J) Quantification of the mediolateral width of *dlx3* domain for WT ($n=6$), MZdchs1b ($n=27$) and MZdchs2^{s_{st1}/s_{st1}} ($n=18$), shown by black line. Statistical significance is indicated by *** $p < 0.0001$.

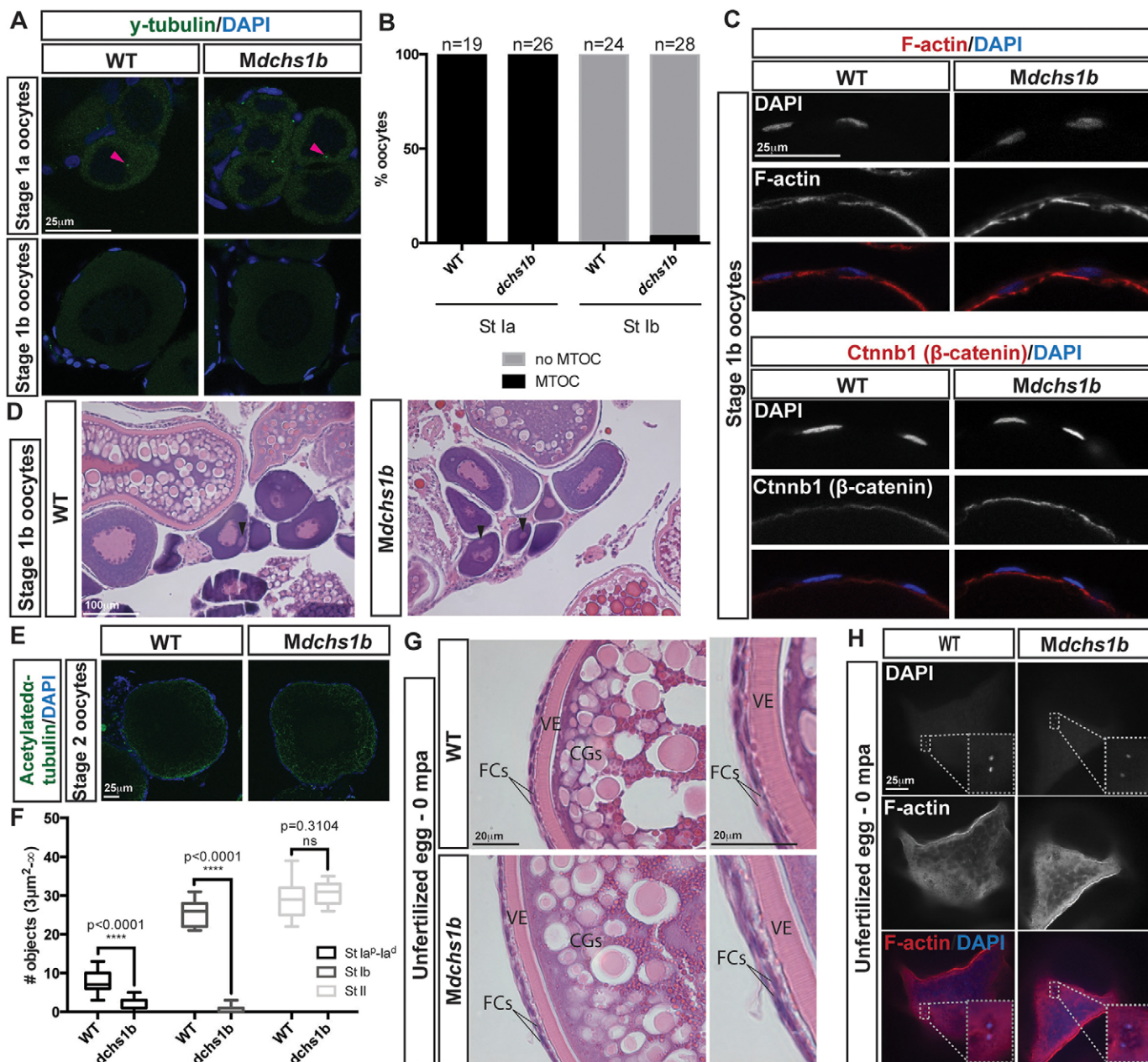


Fig. 2. *dchs1b* oogenesis is largely unaffected. (A) γ -tubulin immunostaining reveals a perinuclear MTOC (pink arrowhead) in the stage Ia oocyte that is lost during stage Ib of oogenesis in WT and *dchs1b* mutants. (B) Quantification of MTOC in oocytes from two WT and three mutant ovaries. (C) Rhodamine Phalloidin labels actin filaments in the cortical ooplasm and in the follicle cell layer. β -catenin localizes to the oocyte cortex or membrane in stage Ib oocytes. (D) H&E-stained ovary sections of WT and *Mdchs1b* ovaries reveal normal polarization of stage Ib oocytes as indicated by the presence of the Balbiani body (black arrowheads). (E) WT and *Mdchs1b* mutant stage II oocytes stained with antibody against acetylated α -tubulin. (F) Quantification of acetylated microtubules from five WT and seven mutant ovaries. (G) H&E-stained ovary sections reveal cortical granule movement toward the cortex, structure of the vitelline envelope (VE) and the two layers of somatic follicle cells surrounding stage III oocytes of WT and *Mdchs1b* mutants. CGs, cortical granules; FCs, follicle cells. (H) F-actin labeling of polar bodies in unfertilized eggs fixed at 0 mpa, with completion of meiosis indicated by the appearance of the polar body and the pronucleus from WT and *Mdchs1b* mutant eggs.

appeared largely normal in *dchs1b* mutant oocytes. Microtubule-organizing centers (MTOCs) were present at stage Ia and lost by stage Ib in WT and mutant oocytes (Fig. 2A,B). Apical basal polarity of follicle cells shown by F-actin and β -catenin enrichment on the follicle cell surface juxtaposed to the oocyte was comparable between WT and mutant stage Ib oocytes (Fig. 2C; supplementary material Fig. S2E). Moreover, the presence of a single Balbiani body in stage Ib and II oocytes of WT and mutants indicated that *dchs* mutant oocytes are polarized (Fig. 2D; supplementary material

Fig. S2F). The number of acetylated α -tubulin-labeled microtubules in stages Ia and Ib was significantly reduced in mutant oocytes compared with WT but by stage II was comparable (Fig. 2E,F; supplementary material Fig. S2G). In unactivated and unfertilized WT and *Mdchs1b* mutant eggs, vitelline envelope morphology, CG size, number and distribution at the cortex were comparable (Fig. 2G). Last, as in WT, polar bodies were extruded from mutant eggs (Fig. 2H). Taken together, these data indicate that *Dchs1b* is dispensable for zebrafish oogenesis.

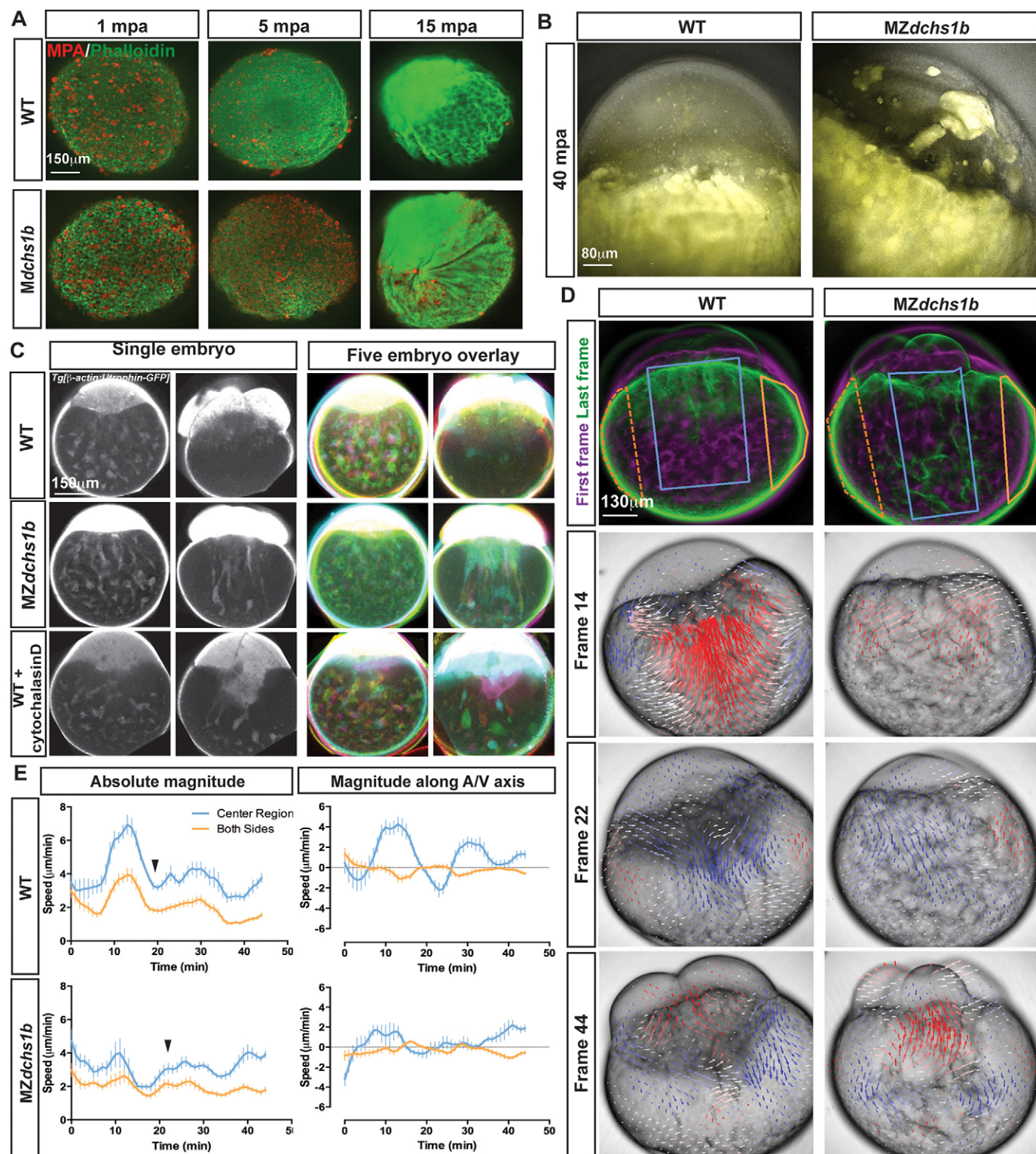


Fig. 3. Egg activation defects in MZdchs1b and cytochalasin D-treated WT embryos. (A) Maximum z-projection of phalloidin (green) and MPA (red) staining of activated WT and M or MZdchs1b eggs fixed at 1, 5 and 15 mpa. (B) Overlay of bright-field and auto-fluorescent maximum z-projections of WT, MZdchs1b eggs at 40 mpa. (C) Single z-plane images from time-lapse movies of single embryos in grayscale, and overlay of five pseudo-colored WT *Tg[β-actin:Utrophin-GFP]*, MZdchs1b; *Tg[β-actin:Utrophin-GFP]* and WT *Tg[β-actin:Utrophin-GFP]* +3 µg/ml cytochalasin D-treated embryos at 15 mpf and 75 mpf. (D) Maximum z-projection images from time-lapse movies of WT, and MZdchs1b embryos in bright-field at frames 14, 22 and 44 with PIV analysis overlaid. PIV analysis: red arrows, towards the animal pole; blue arrows, towards the vegetal pole; arrow length indicates movement magnitude. Leftmost panels: pseudo-colored first frame (magenta) and last frame (green) overlaid. (E) Quantification of cytoplasmic movement with PIV for WT ($n=8$) and MZdchs1b ($n=9$) embryos. Blue lines represent center of embryos marked by blue boxes in left panels in D, and orange lines represent both edges of embryos demarcated by orange crescent boxes in D. Left graphs show magnitude of motion and right graphs show magnitude of motion with respect to embryonic A/V axis. Graphs are plotted with s.d. bars.

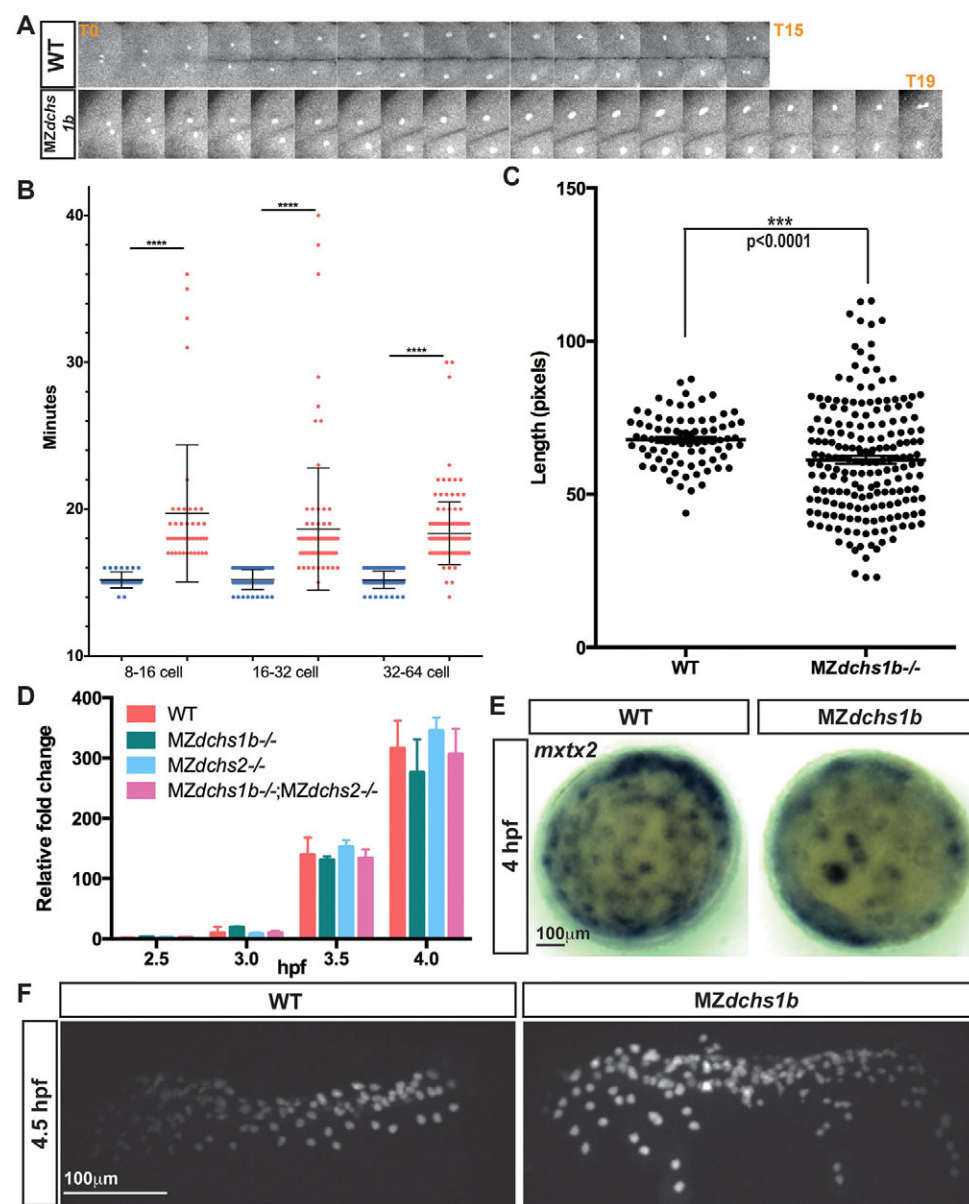


Fig. 4. Uncoupling of cell division and MBT in MZdchs1b mutants. (A) One-cell division from early anaphase to the next early anaphase in WT and MZdchs1b blastula-stage embryos. (B) Quantification of length of cell divisions in WT (blue) and MZdchs1b (red) embryos. (C) Quantification of length of the longest cell axis in 128-cell-stage WT and MZdchs1b embryos. (D) Zygotic expression of boz in MZdchs1b, MZdchs2^{st1/st1} and MZdchs1b^{fh275/fh275};MZdchs2^{st1/st1} mutants compared with WT relative to MBT. (E) mxtx2 WISH in time-matched WT and MZdchs1b embryos, labeling YSN at 4 hpf; animal-pole view. (F) H2B-GFP labeling of YSN in WT and MZdchs1b embryos.

Delayed CGE in Mdchs1b mutants

Upon activation, delayed CGE in *Mdchs1b* mutant eggs was evident from stereomicroscopic analysis (data not shown). We next labeled CGs in fixed eggs using fluorescent dye-conjugated *Maclura pomifera* agglutinin (MPA) (Becker and Hart, 1999; Dosch et al., 2004; Mei et al., 2009; Talevi et al., 1997). At 1 min post activation (mpa), CGE in WT and *Mdchs1b* eggs were comparable. By 5 mpa, WT eggs had largely completed CGE, whereas CGs persisted in mutant eggs until ~15 mpa (Fig. 3A). Consistent with delayed CGE, chorion expansion in mutants was delayed relative to WT (supplementary material Movie 1). As histological analysis of ovaries revealed no overt differences between CG formation or distribution in WT and *Mdchs1b* oocytes (Fig. 2H; supplementary material Fig. S2F), we conclude that maternal *dchs1b* function promotes CGE during egg activation.

dchs1b function is required for actin-dependent separation of yolk and cytoplasm

Several lines of evidence implicate maternal *Dchs1b* function in cytoplasmic streaming. First, in the blastodisc of cleavage-stage

MZdchs1b mutants, we observed amorphous yolk masses (Fig. 1F), which were apparent by yolk autofluorescence (Fig. 3B). Second, visualizing F-actin using *Tg[β-actin:utrophin-GFP]* (Behrndt et al., 2012) revealed cytoplasm persisting within the yolk of mutants at 75 mpf, when most of the actin-containing cytoplasm had segregated into the blastodisc of WT embryos (Fig. 3C,D). Third, spinning-disk confocal time-lapse microscopy and particle image velocimetry (PIV) analysis (Prasad and Jensen, 1995; Yin et al., 2008) of internal movements of the cytoplasm during egg activation in WT revealed periods of robust animal-ward movements at the blastodisc yolk cell interface punctuated by smaller fluctuations towards the vegetal pole, reminiscent of ebb and flow motion (Fig. 3D; supplementary material Movie 2). The initial surge of animal-ward movement in central regions of WT embryos at 30 mpf averaged 7 μm/min and was mirrored by smaller 3 μm/min vegetal-ward movements at the cortex, followed by smaller ebb and flow movements (Fig. 3E). The vigorous movements appeared well-organized with two centers of circular motion, which we interpret as a circular, toroidal movement within the yolk (Fig. 3D). All movements were of smaller amplitude in *MZdchs1b* mutants, with

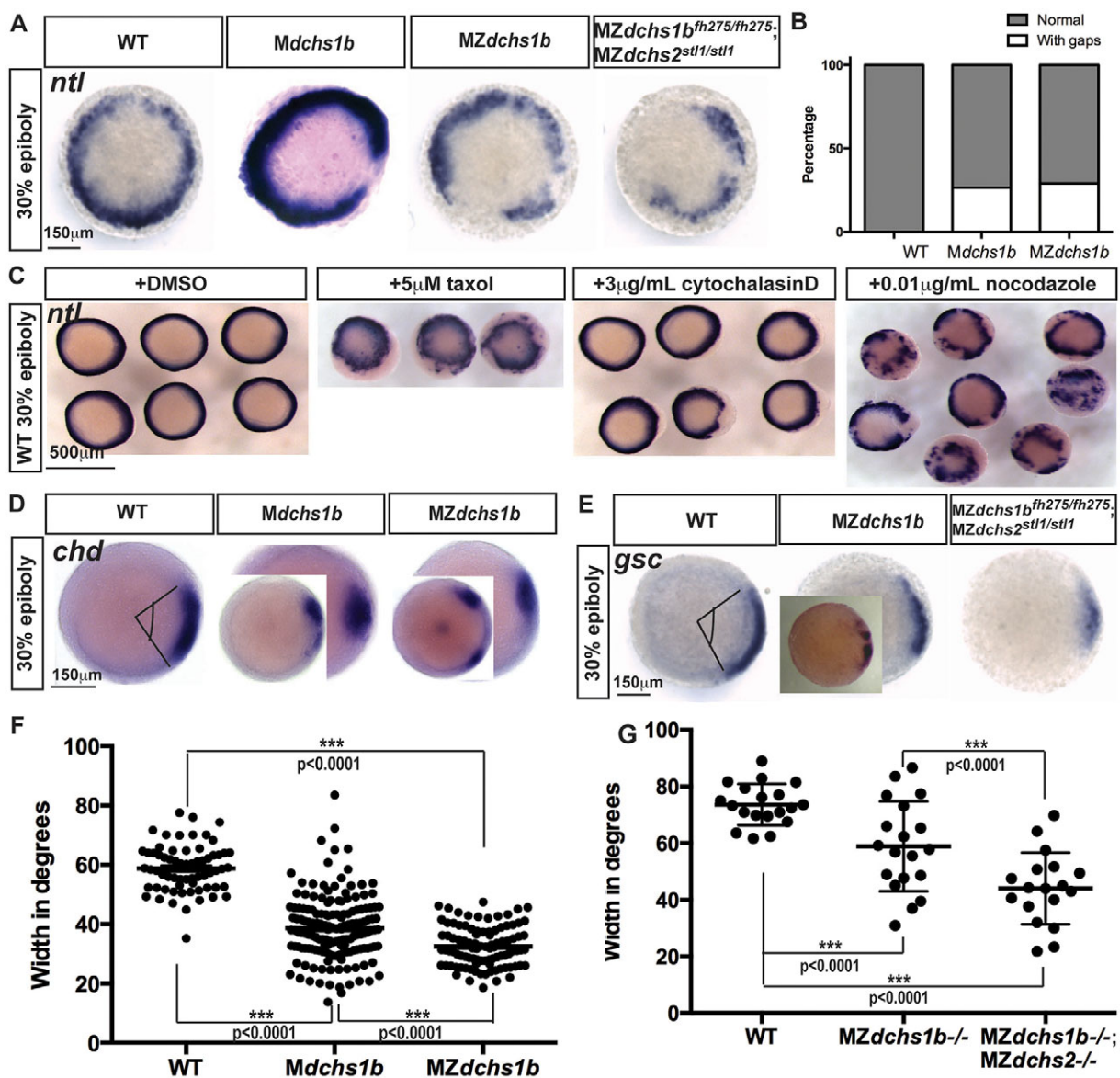


Fig. 5. Mesoderm specification is deficient in *MZdzchs1b* embryos and WT embryos with impaired cytoskeleton. (A) *ntl* expression in *MZdzchs1b*, *Mdzchs1b* and *MZdzchs1b^{fh275/fh275}; MZdzchs2^{stl1/stl1}* stage-matched embryos at 30% epiboly; animal-pole view. (B) Quantification of gaps in *ntl* expression in WT, *Mdzchs1b* and *MZdzchs1b* embryos. (C) *ntl* expression in WT embryos treated with DMSO, 5 μM taxol, 3 μg/ml cytochalasin D and 0.01 μg/ml nocodazole at 30% epiboly; animal-pole view. (D) *chd* expression domain in WT, *Mdzchs1b* and *MZdzchs1b* embryos. Insets show embryos with gap in expression domain. (E) *gsc* expression in WT, *Mdzchs1b*, *MZdzchs2^{stl1/stl1}* and *MZdzchs1b^{fh275/fh275}; MZdzchs2^{stl1/stl1}* stage-matched embryos at 30% epiboly; animal-pole view. Inset in *MZdzchs1b* panel shows representative image of disrupted *gsc* domain. (F) Measurement of the *chd* expression domain in degrees for embryos shown in D. (G) Measurement of the *gsc* expression domain in degrees for embryos shown in E.

the maximum being 4 μm/min, the organized toroidal movements were lost and coordination of central movements and cortical flow was impaired (Fig. 3D,E; supplementary material Movie 3). The ooplasmic streaming abnormalities and delayed CGE, as well as bundled actin later in development (supplementary material Fig. S4E), imply actin cytoskeleton deficits in *MZdzchs1b* mutants, as both processes rely on F-actin dynamics (Becker and Hart, 1999).

Delayed and abnormal cleavages with normal aspects of MBT in *MZdzchs1b* mutants

Time-lapse analyses also revealed delayed and non-uniform cleavages in *MZdzchs1b* mutants. Quantification of cleavage cycle length from anaphase to anaphase revealed an average of 15 min in

WT embryos, compared with, on average, 19 min and up to 40 min in *MZdzchs1b* mutants (Fig. 4A,B). In addition to longer cleavage cycles, *MZdzchs1b* mutants displayed abnormal cleavage patterns, such that cells divided into three or more daughters, yielding differently sized blastomeres (Fig. 4C; supplementary material Movies 4 and 5).

To determine whether subsequent developmental processes were delayed in *MZdzchs1* mutants, we analyzed MBT onset, marked by activation of zygotic transcription, appearance of YSL nuclei (YSN) and loss of cell division synchrony (Kane and Kimmel, 1993). Surprisingly, qRT-PCR revealed comparable expression onset for several zygotic genes, including *boz/dharma*, *bmp2b*, *sqt*, *cyc* and *chordin* (Schulte-Merker et al., 1997; Sirotkin et al., 2000; Solnica-Krezel and Driever, 2001; Yamanaka et al., 1998) between WT and

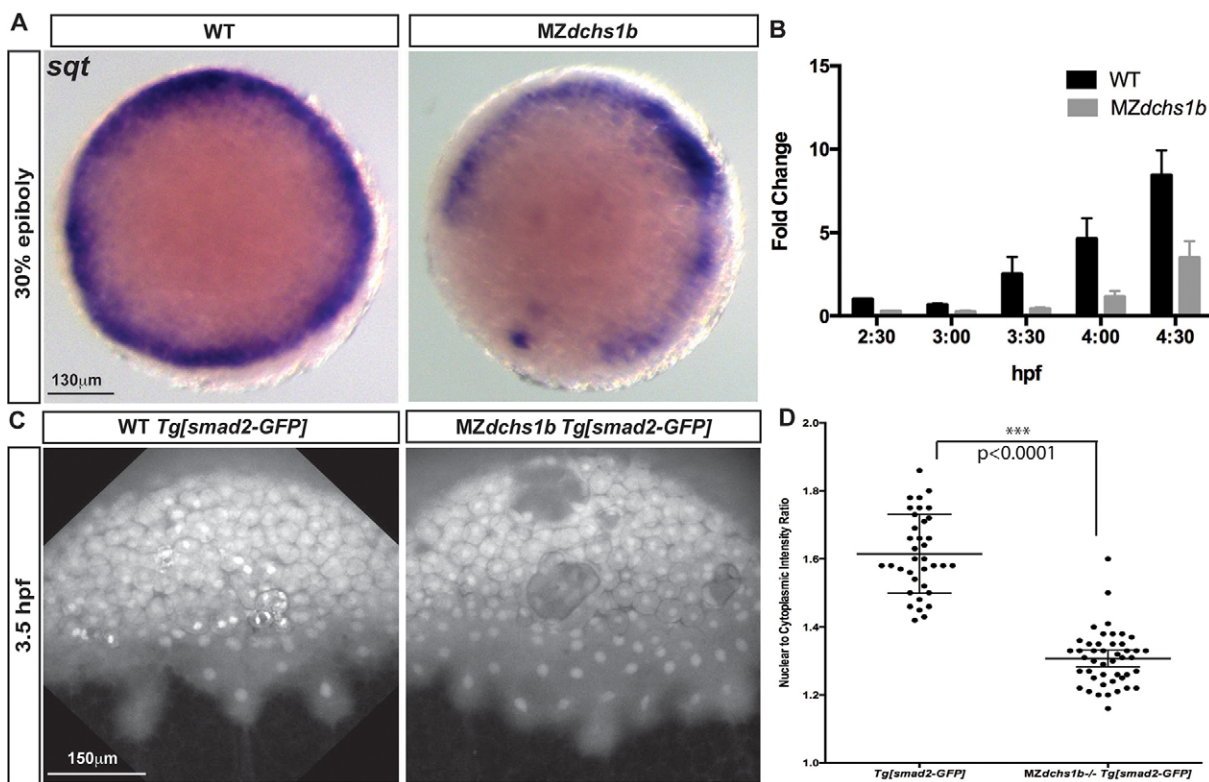


Fig. 6. Reduced Nodal signaling in MZdchs1b embryos. (A) *sqt* expression in stage-matched WT and MZdchs1b embryos; animal-pole view. (B) Quantitative RT-PCR of *sqt* RNA in time-matched WT and MZdchs1b embryos during MBT. (C) Max z-projection of time-matched WT *Tg[smad2-GFP]* and MZdchs1b; *Tg[smad2-GFP]* embryos at 3.5 hpf. (D) Quantification of nuclear-to-cytoplasm ratio for GFP intensity in WT *Tg[smad2-GFP]* and MZdchs1b; *Tg[smad2-GFP]* embryos shown in C.

MZdchs1b mutants (Fig. 4D and Fig. 6B; supplementary material Fig. S3A,B,E). Upon YSL formation, the YSN undergo several divisions and spread towards the animal and vegetal poles (D'Amico and Cooper, 2001; Solnica-Kreuzel and Driever, 1994). YSN appeared on time in MZdchs1b mutants, although their distribution revealed by *mxtx2* (Hong et al., 2011) or H2B-GFP labeling was abnormal, compared with uniformly spaced YSN in WT (Fig. 4E,F). Hence, although MZdchs1b mutants appeared morphologically younger than age-matched WT embryos, aspects of MBT occurred on time.

Abnormal Nodal signaling in MZdchs1b mutant blastulae

The YSL is a source of signals that induce and pattern germ layers (Carvalho et al., 2009; Chen and Kimelman, 2000; Fekany et al., 1999; Mizuno et al., 1999; Yamanaka et al., 1998). Given the abnormal YSN distribution in MZdchs1b mutants, we investigated YSL-mediated inductive events. The pan-mesodermal marker *ntl* (Schulte-Merker et al., 1994) was detected at 30% epiboly in a continuous ring around the blastoderm margin in WT, but the *ntl* domain was punctuated by gaps in ~30% of *Mdchs1b* and MZdchs1b embryos (Fig. 5A,B). The gastrula organizer markers *chordin* (*chd*) and *goosecoid* (*gsc*) were expressed in an arc of 60° and 75°, respectively, in WT, whereas both domains were significantly reduced or interrupted in MZdchs1b mutants (Fig. 5D-G). In WT gastrulae, *sox17* expression marks endodermal precursors and dorsal forerunner cells (Alexander and Stainier, 1999; Engleka et al., 2001; Hudson et al., 1997). Mutants had fewer *sox17*-expressing endodermal cells, and the forerunner cell domain was vegetally displaced relative to the blastoderm margin and fragmented (supplementary material Fig. S3C).

As both mesendoderm and the Nieuwkoop center were aberrant in MZdchs1b mutants (Fig. 5A-G), we investigated the signals inducing them. Nodal morphogens induce mesodermal and endodermal tissues in a concentration-dependent manner (Agius et al., 2000; Chen and Schier, 2001; Erter et al., 1998; Gritsman et al., 2000; Jones et al., 1995). Transcripts of the Nodal signaling ligands *cyclops* (*cyc*) and *squint* (*sqt*) were expressed in a continuous ring at the blastoderm margin of 30% epiboly WT blastulae (Chen and Schier, 2001; Erter et al., 1998; Feldman et al., 1998; Sampath et al., 1998), and discontinuous domains in MZdchs1b mutants (Fig. 6A; supplementary material Fig. S3D). Consistently, qRT-PCR revealed significantly reduced abundance of both *cyc* and *sqt* transcripts in MZdchs1b compared with WT (Fig. 6B; supplementary material Fig. S3E). To assess Nodal signaling functionally, we analyzed nuclear accumulation of the transcription factor Smad2 (Saka et al., 2007; Schier and Shen, 2000). Using the *Tg[β-actin:smad2-GFP]* transgene reporter of Nodal activity *in vivo* (Dubrulle et al., 2015), we observed a significantly reduced ratio of nuclear-to-cytoplasmic Smad2-GFP in MZdchs1b blastulae compared with WT (Fig. 6C,D). Together, these results indicate that reduced Nodal signaling partially accounts for the mesendodermal and Nieuwkoop center deficits of MZdchs1b embryos.

Impaired *wnt8a* RNA translocation in MZdchs1b mutants

Nieuwkoop center formation requires microtubule-dependent asymmetric transport of DDs, such as *wnt8a* mRNA, from the vegetal pole to the future dorsal side of the embryo (Ge et al., 2014; Gore and Sampath, 2002; Jesuthasan and Strähle, 1997; Lu et al., 2011; Nojima et al., 2010; Shao et al., 2012; Tran et al., 2012).

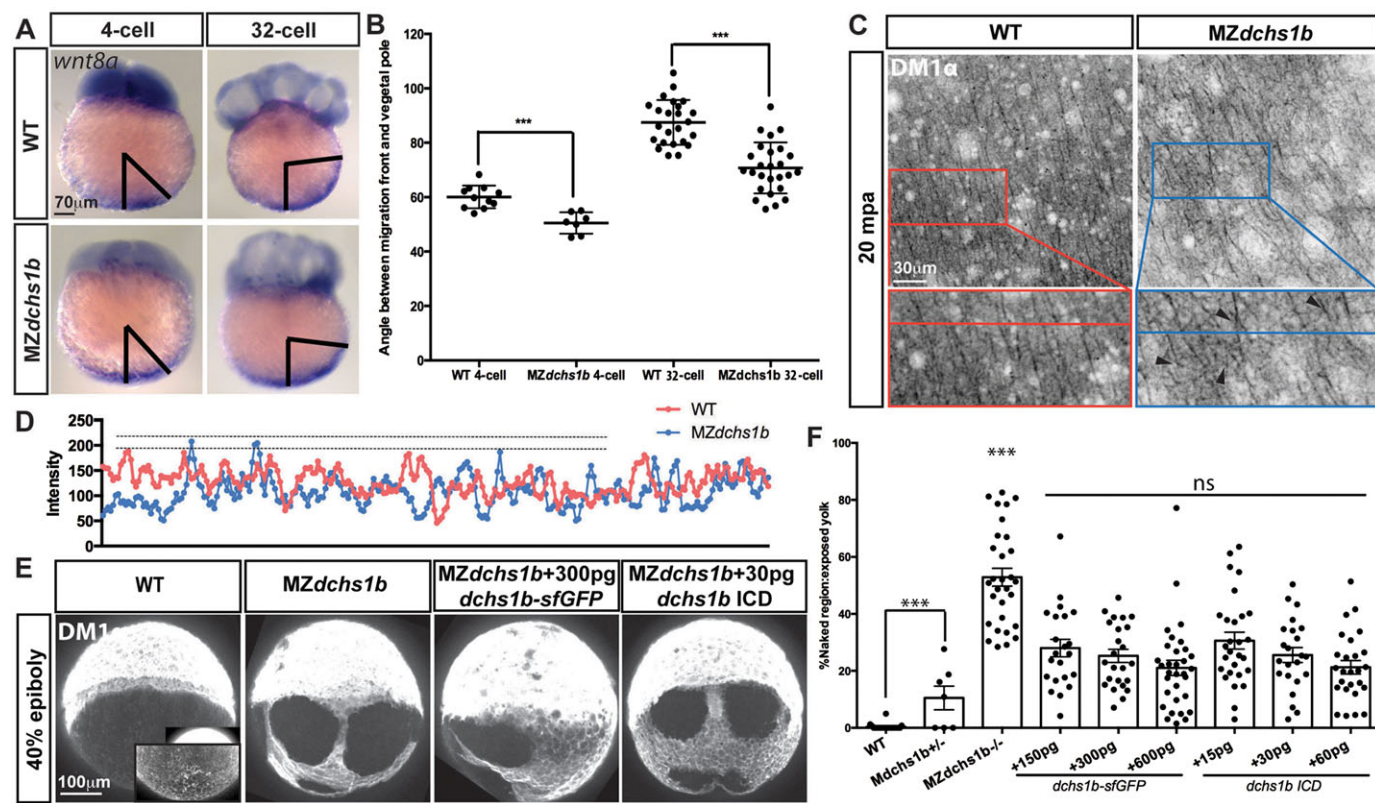


Fig. 7. Abnormal *wnt8a* expression-domain shift and vegetal microtubule populations in *MZdchs1b* mutants, and *dchs1b* RNA rescue of the microtubule phenotype. (A) *wnt8a* expression in WT and *MZdchs1b* embryos at four- and 32-cell stages. Black bars mark the angle between the edge of *wnt8a* expression domain from the vegetal pole. (B) Quantification of the angle between the edge of the *wnt8a* expression domain and the vegetal pole for WT and *MZdchs1b* embryos at four- and 32-cell stages. *** $P<0.005$. (C) DM1 α labeling of vegetal-pole microtubules for WT and *MZdchs1b* embryos at 20 mpa. Top panels show parallel microtubule arrays in tangential view of embryos. Bottom panels show higher magnification views, with black arrowheads indicating crossing microtubules. (D) Plot profile of WT and *MZdchs1b* parallel arrays for intensity. (E) DM1 α labeling of microtubules in WT, *MZdchs1b* and *MZdchs1b* embryos injected with *dchs1b* full-length RNA and ICD RNA at 40% epiboly. (F) Quantification of rescue-of-yolk microtubule phenotype, with different doses of *dchs1b* full-length or ICD RNAs. *MZdchs1b* is statistically different from all other conditions. ns, not significant; *** $P<0.0001$.

WISH revealed proper vegetal pole localization of *wnt8a* transcripts in unactivated *Mdchs1b* eggs (supplementary material Fig. S4A). However, animal-ward translocation of *wnt8a* RNA following fertilization was reduced in *MZdchs1b* embryos compared with WT (Fig. 7A,B). Moreover, in some embryos, *wnt8a* expression expanded symmetrically (supplementary material Fig. S4A).

wnt8a mRNA transport is mediated by microtubules, which, after egg activation, form transient parallel arrays aligning with the future dorsal side of the embryo (Lu et al., 2011; Tran et al., 2012). Therefore, we hypothesized that impaired transport of *wnt8a* in *MZdchs1b* embryos was due to microtubule abnormalities. Visualizing microtubules with the DM1 α antibody in immunofluorescence and using *Tg[XlEf1a1:dcl2-GFP]*, we observed parallel arrays of microtubules that appeared misoriented in mutants, crossing each other (Fig. 7C; supplementary material Fig. S4C) and were more bundled, as evidenced by higher intensity in *Mdchs1b* mutants compared with WT (Fig. 7D). Progressive bundling resulted in dramatically different appearances of vegetal microtubules during gastrulation (Fig. 7E; supplementary material Fig. S4D). Notably, microtubule bundling could be partially rescued by injection at one-cell stage of synthetic RNAs encoding either full-length *Dchs1b*-sfGFP or *Dchs1b* intracellular domain (Fig. 7E,F). We posit that these vegetal microtubule abnormalities in *MZdchs1b* mutants could impede translocation of *wnt8a* transcripts, consequently resulting in Nieuwkoop center and gastrula organizer deficiencies (Fig. 5D-G).

Disrupting cytoskeleton dynamics in WT embryos phenocopies *MZdchs1b* mutant defects

We employed a pharmacological approach to determine whether specifically targeting actin or microtubules could phenocopy *MZdchs1b* defects. Partial disruption of the F-actin network (supplementary material Fig. S5A) of *Tg[β-actin:utrophin-GFP]* embryos using 3 μ g/ml of cytochalasin D in the medium from activation (Cooper, 1987; Leung et al., 2000; Schliwa, 1982) impeded yolk/cytoplasm segregation similar to *MZdchs1b* mutants. Globular yolk inclusions occupied the blastodisc, while cytoplasmic islands remained in the yolk at 75 mpf (Fig. 3C). At 10–15 μ g/ml of cytochalasin D, CGE was perturbed, chorions did not fully expand, cytoplasmic streaming was blocked (supplementary material Fig. S5B) and development arrested. We then assessed the effect of 3 μ g/ml cytochalasin D treatment on mesodermal specification and found that a fraction of treated embryos had uneven *ntl* marginal domains and reduced *gsc* expression domains, similar but milder phenotypes than those in *MZdchs1b* mutants (Fig. 5C; supplementary material Fig. S5C).

Next, we perturbed microtubule dynamics using nocodazole to prevent tubulin polymerization, or taxol to stabilize microtubules (Heidemann et al., 1980). Culturing WT embryos in 0.001, 0.002 and 0.005 μ g/ml of nocodazole or 5 μ M taxol from 10 mpa did not affect cytoplasmic streaming during egg activation. Microtubule-inhibiting drugs were added at 1 hpf to test the effect on mesoderm formation to avoid interference with initial *wnt8a* translocation. The

treated embryos had punctuated marginal *ntl* domains and smaller or fragmented *gsc* domains, phenocopying *MZdchs1b* mutant defects (Fig. 5C; supplementary material Fig. S5D). In embryos cultured with 0.002 µg/ml and 0.005 µg/ml nocodazole, *ntl* expression was reduced to one side of the embryo and *gsc* expression was absent (supplementary material Fig. S5D). Surprisingly, taxol caused similar defects in mesoderm formation in WT embryos, suggesting that changing the dynamics of microtubules, whether destabilizing or stabilizing, produced *MZdchs1b*-like phenotypes (Fig. 5C; supplementary material Fig. S5C,D). Based on the similar defects observed in *MZdchs1b* mutants and pharmacological disruption of microtubule and/or actin cytoskeletons in WT, the abnormal microtubule and actin networks in mutants (Fig. 3C and Fig. 7C), and rescue of microtubule bundling by expressing *Dchs1b* (Fig. 7E,F), we propose that *Dchs1b* regulates the dynamics of the actin and/or microtubule networks to promote egg activation and early patterning.

DISCUSSION

Here, we have identified novel roles for *Dchs1b* in early patterning and morphogenesis at the earliest stages of zebrafish development, the transcriptionally silent egg and blastula, without perceivable defects in oogenesis. *Drosophila Dachsous* functions as a Fat ligand to regulate growth through Hippo signaling, planar polarity and cell-cell adhesion in epithelial tissues (Casal et al., 2006; Clark et al., 1995; Ishiuchi et al., 2009; Rawls et al., 2002; Strutt and Strutt, 2002; Yang et al., 2002). In PCP regulation, Dachsous is proposed to be instructive in promoting polarity of apical microtubule arrays that mediate asymmetric transport of core PCP proteins (Harumoto et al., 2010; Matis et al., 2014). The essential function of *Dchs1b* in vertebrate development was revealed by pleiotropic phenotypes and postnatal lethality of *Dchs1* knockout mice (Mao et al., 2011; Zakaria et al., 2014). Furthermore, in humans, *DCHS1* mutations can lead to a recessive syndrome characterized by pleiotropic phenotypes including periventricular neuronal heterotopia (Cappello et al., 2013). However, the cellular mechanisms via which *Dchs* affects vertebrate development are unknown. We propose that in zebrafish zygotes and early embryos, *Dchs1b* coordinates CGE, cytoplasmic segregation and maternal mRNA translocation by regulating the organization and dynamics of the actin and microtubule cytoskeleton, probably via a Fat- and PCP-independent mechanism. Indeed, the MZ PCP pathway mutants *trilobite/vangl2* and *knypek/glypican4* do not exhibit such early developmental defects (Ciruna et al., 2006; Topczewski et al., 2001).

Zebrafish *MZdchs1b* and *MZdchs2* mutants afforded assessment of the earliest *dchs* functions in embryogenesis. Correlated with its strong maternal expression, only *MZdchs1b* embryos exhibited pre-MBT phenotypes (Fig. 1). That two independent nonsense alleles manifest the same spectrum of phenotypes and that *dchs1b* RNA rescued abnormal microtubule organization in the YSL provides evidence that the observed phenotypes are due to loss of *dchs1b* function. The variable penetrance and expressivity of *MZdchs1b* phenotypes is typical of other zebrafish maternal and MZ mutants, such as *ichabod/β-catenin2*, *bozozok* and *squint* (Fekany et al., 1999; Kelly et al., 2000; Sirotnik et al., 2000). Functional redundancy between the three *dchs* genes is supported by reduced phenotypic variability and increased phenotypic severity in *MZdchs1b^{fh275/fh275};MZdchs2^{stl1/stl1}* compound mutants (Fig. 1F and Fig. 5A,E,G).

A striking finding is the essential role *Dchs1b* plays in the single-celled egg and early zygote. *Mdchs1b* mutants showed delayed

CGE and incomplete cytoplasmic segregation (Fig. 3). These egg-activation processes occur minutes after an egg is laid and are independent of fertilization, transcriptional activity and cell-cell interactions. Based on our histological findings these defects are proximal to *Dchs1b* rather than reflecting abnormalities during oogenesis. First, hallmarks of oocyte/egg polarity examined were normal in *Mdchs1b* mutants (Fig. 2; supplementary material Fig. S2E-G): Balbiani bodies were present, a single cytoplasmic island and single micropyle occupied the animal pole, and *wnt8a* maternal mRNA was localized at the vegetal pole. Additionally, CGs translocated to the cortex and polar bodies were extruded normally. However, as we did not examine every aspect of oogenesis, the possibility of *Dchs*-mediated intercellular interactions during early oogenesis cannot be fully ruled out. These analyses indicate that egg activation processes, which are dependent on dynamics of actin or microtubule cytoskeleton, become defective in M or *MZdchs1b* mutants after activation/fertilization of the egg. The observation that injection of synthetic RNA encoding *Dchs1b* intracellular domain rescued abnormal organization of the microtubule network in the syncytial yolk cell (Fig. 6E,F) further strengthens the notion that *Dchs1b* has activities independent of intercellular interactions with Fat. This contrasts with all previous studies that implicated Dachsous in multicellular or tissue contexts, where Dachsous functions through heterophilic intercellular interactions with Fat (Casal et al., 2006; Clark et al., 1995; Ishiuchi et al., 2009; Rawls et al., 2002; Strutt and Strutt, 2002; Yang et al., 2002). The consequences of inactivating the maternal *Dchs* function in these systems remain to be investigated.

Our data support a novel *Dchs1b* role in mediating and coordinating multiple processes during early development. During egg activation in M/*MZdchs1b* mutants, CGE and cytoplasmic streaming were both delayed and cytoplasmic streaming was uncoordinated (Fig. 3). During cytoplasmic streaming, actin-dependent movement of cytoplasm between the central and peripheral yolk were uncoordinated and the organized centers of motion present in WT were lost in *MZdchs1b* mutants. Later events that together constitute MBT were disassociated in *MZdchs1b*, with YSL appearance and zygotic transcription initiation of several zygotic genes occurring on time in mutants, despite delayed and uneven maternal cell divisions (Fig. 4). This lack of coordination in *MZdchs1b* mutants is interesting in light of the well-established role for Dachsous in *Drosophila* planar polarity, as, after all, planar polarity entails coordination of cell polarity across a tissue (Goodrich and Strutt, 2011).

Unexpectedly, *MZdchs1b* mutants also displayed dorsal organizer and mesendoderm deficiencies. As the underlying cellular mechanism that leads to *MZdchs1b* phenotypes we implicated defective cytoskeletal dynamics through four non-mutually exclusive models (Fig. 8). First, in the mutant blastodisc, defective cytoplasmic streaming produces ectopic yolk masses (Fig. 3B,C), which later present physical obstacles to cell migration and morphogen diffusion and could reduce Nodal signaling (Fig. 6), leading to mesendoderm deficiencies (Fig. 5). In the current model for Nodal morphogen gradient formation, ligand travels through tissue via diffusion and is hindered by binding and tortuosity created by cells in the tissue (Muller et al., 2013). Second, the transient parallel microtubule arrays were more bundled and misoriented in *MZdchs1b* mutants compared with WT, and maternally deposited *wnt8a* mRNA that is translocated upon fertilization by the microtubule cytoskeleton (Lu et al., 2011; Tran et al., 2012) displayed abnormal distribution after fertilization (Fig. 7A,B). Therefore, abnormal organization and function of microtubules in

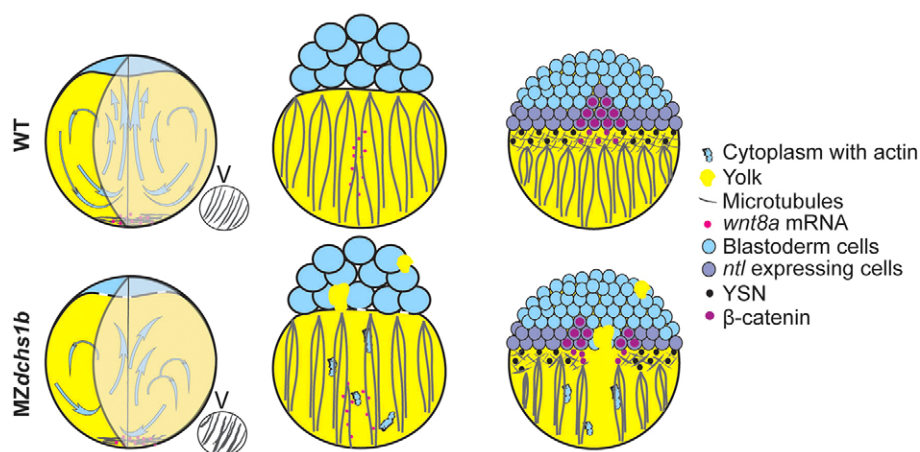


Fig. 8. Model for Dchs1b function during early embryogenesis. (Left) MZdchs1b mutants show uncoordinated movement of actin containing cytoplasm, leading to incomplete yolk-cytoplasm segregation. Insets show vegetal views of parallel array microtubules. (Middle) Dorsal view, transport of dorsal determinant is abnormal in MZdchs1b mutants; mutant blastoderm retains yolk while cytoplasm is present in the yolk cell. (Right) MZdchs1b mutant gastrula displays defects in YSN organization, microtubule bundling and mesoderm, irregular β -catenin nuclear distribution and organizer gene expression.

MZdchs1b mutants could lead to impaired dorsal determinant translocation, thereby affecting β -catenin nuclear localization (supplementary material Fig. S4C), and, consequently, β -catenin-dependent zygotic gene expression in the Nieuwkoop center and dorsal mesoderm, such as *sqt*, *gsc* and *ntl* (Fig. 5) (Schulte-Merker et al., 1994; Schier and Shen, 2000; Chen and Schier, 2001; Erter et al., 1998; Feldman et al., 1998). Third, as the dorsal YSL is the initial source of Nodal signaling at the onset of MBT (Chen and Kimelman, 2000), the disorganized microtubule cytoskeleton and YSN on the dorsal side of MZdchs1b blastulae, where nuclear β -catenin initially accumulates (Kelly et al., 2000), might compromise Nodal signaling as well. Last, a model for mechanical induction of mesoderm and phosphorylation of β -catenin due to physical stress caused by epiboly has been recently proposed (Brunet et al., 2013). The hyperbundled cytoskeleton (Fig. 7E; supplementary material Fig. S4D,E) in MZdchs1b yolks could lead to differential stress at the blastoderm margin, contributing to mesoderm deficiencies. All these mechanisms could contribute to the variable defects seen in MZdchs1b mutants (Fig. 8).

The abnormalities seen in *Mdchs1b* and MZdchs1b embryos can be traced back to defects in cytoskeletal dynamics. We posit that Dchs1b regulates both the actin and microtubule cytoskeletal systems independently, as perturbation of either in WT embryos phenocopied unique subsets of mutant defects: e.g. perturbing actin but not microtubules led to defects in cytoplasmic streaming. In *Drosophila*, Dachsous regulates the unconventional myosin Dachs (Cho and Irvine, 2004; Mao et al., 2006); however, its vertebrate homolog remains to be identified. Additionally, Dachsous regulates dynamics of non-centrosomal microtubules in *Drosophila*, where both alignment and asymmetric distribution are affected in mutants (Harumoto et al., 2010; Matis et al., 2014). However, how Dachsous interacts with and regulates microtubules remains unknown. Identification of molecular links between Dchs and the cytoskeleton in vertebrates is an important future goal.

We have discovered an essential role for Dchs1b during early vertebrate morphogenesis and cell-fate specification through regulation of the actin and microtubule cytoskeleton. However, it remains to be determined whether all MZdchs1b mutant defects can be explained by the loss of Dchs1b regulation of the cytoskeleton in the affected processes, or whether some are secondary to earlier abnormalities. We found that both MZdchs1b and MZdchs2^{stl1/stl1} mutant embryos display C&E defects during gastrulation, but whether Dchs achieves this by influencing PCP in zebrafish gastrula is unclear. Additionally, we observed no overt growth defect in MZdchs1b mutants as in *Drosophila*, where Ds regulates the Hippo

pathway (Cho et al., 2006). However, we have not ruled out tissue-specific growth and morphogenesis defects later in development, as zebrafish *dchs2* morphants have been shown to display craniofacial defects (Le Pabic et al., 2014). Recent studies show an intriguing relationship between cell polarity and fate with Hippo signaling in the mouse blastocyst (Anani et al., 2014; Hirate et al., 2013; Kono et al., 2014). Moreover, Hippo signaling pathway components can modulate the Wnt/ β -catenin pathway in multiple contexts, including the *Drosophila* wing imaginal disk, and murine kidney and heart (Baena-Lopez et al., 2008; Heallen et al., 2011; Imajo et al., 2012; Varelas et al., 2010). Furthermore, the Hippo pathway can both regulate and respond to the actin cytoskeleton during collective cell migration and cell polarization (Bertrand et al., 2014; Low et al., 2014; Lucas et al., 2013). These studies pose a fascinating web of possible genetic and functional interactions for Dchs in other developmental processes. Answering the question of how Dchs functions during development will reveal which roles are conserved from *Drosophila* to vertebrates and will shed light on how it leads to pleiotropic phenotypes in patients with Van Maldergem syndrome.

MATERIALS AND METHODS

Zebrafish lines

AB, *Tg[XIEef1a1:dclk2-GFP]*, *Tg[β-actin:utrophin-GFP]* and *Tg[β-actin:smad2-GFP]* (Campinho et al., 2013; Tran et al., 2012) lines were used. TILLING to generate *dchs1b*^{flh274} and *dchs1b*^{flh275} and *dchs2*^{stl1} mutations was performed as described (Draper et al., 2004). This study was performed in strict accordance with the recommendations in the Guide for the Care and Use of Laboratory Animals of the National Institutes of Health. All procedures and experimental protocols approved by the Animal Studies Committees of Harvard University, Fred Hutchinson Cancer Research Center, Albert Einstein College of Medicine and Washington University School of Medicine.

Embryo staging and maintenance

In vitro fertilization was used to generate time-matched WT and mutant embryos, the age of which is reported as hours post fertilization (hpf). Stage-matched mutant and WT embryos were collected from pairwise crosses that spawned within 10 min of each other and were matched by morphological landmarks at the time of the experiment (Kimmel et al., 1995). Embryos were kept in egg water (60 µg/ml Instant Ocean in distilled water) at 28.5°C.

Live imaging

Cyttoplasmic streaming

WT and *Mdchs1b* eggs were fertilized *in vitro*, activated in egg water for 8 min at room temperature (RT), manually dechorionated and mounted in 0.3–0.5% low-melting-temperature agarose (LMA; Seaplaque, catalog

number 50100) in $0.3\times$ Danieau's buffer on a round #1 coverglass bottom dish. z -stack time-lapses were collected using a spinning-disk confocal microscope (SDCM; Olympus IX81, Quorum) in bright-field with a $10\times$ objective, from 14–59 mpf. Each step in the z -stack was $3\text{ }\mu\text{m}$ and the entire stack was 55 slices, with stacks collected every minute.

Vegetal microtubules

Tg[XlEefla1:dclk2-GFP] and *Mdchs1b*; *Tg[XlEefla1:dclk2-GFP]* embryos were collected within three minutes of each other, manually dechorionated and mounted as above. z -stack time-lapses were collected using SDCM with a 491-nm wavelength laser at $10\times$, with z -slice of $3\text{ }\mu\text{m}$ and 51 z -slices from 0.5 to 6.5 hpf every 3 min, or at $40\times$, with z -slice of $0.5\text{ }\mu\text{m}$ and 33 slices from 15 to 30 mpa every minute.

Autofluorescence of yolk

WT and *Mdchs1b* 40 mpa embryos were mounted as described above. z -stacks were collected with SDCM with a 491-nm wavelength laser and DIC at $10\times$ with z -slices of $3\text{ }\mu\text{m}$.

Cell division

Embryos were injected with 70 pg of *H2B-GFP* RNA at one-cell-stage and counterstained with CellTrace Bodipy (C34556) at 1:100. z -stacks were collected at 1 hpf with SDCM with 491 and 561 nm wavelength lasers at $10\times$ with z -slices of $3\text{ }\mu\text{m}$.

Nuclear labeling of YSL

70 pg of *H2B-GFP* RNA was injected into the YSL around 3 hpf. z -stacks were collected at 4 hpf with SDCM with a 491-nm wavelength laser $10\times$ with z -slices of $3\text{ }\mu\text{m}$.

Immunohistochemistry (IHC)

DAB

Embryos were fixed in 4% paraformaldehyde at 3 hpf, washed in PBS and blocked in 10% FBS in PBSTween. Primary antibody: anti- β -catenin Sigma C7207 (1:250 dilution). The stained embryos were developed using Vectastain ABC vector kit (PK-6102) and ImmPACT DAB kit (SK-4105). Microtubule staining with anti-DM1 α antibody (CALBIOCHEM, #CP06; 1:500 dilution) at 50% epiboly and Alexa Fluor goat anti-mouse secondary antibody (#A11031; 1:500 dilution) was performed according to Gard (1991) with modification by Solnica-Krezel and Driever (1994).

In situ hybridization

Embryos were fixed at various stages in buffer containing 4% paraformaldehyde (PFA), 4% sucrose and 120 μM calcium chloride at 4°C overnight. WISH was performed according to (Thisse and Thisse, 2008).

Quantitative RT-PCR

Each RNA sample was isolated using Trizol (Life Technologies, #15596-026) from 30 WT or mutant embryos. RNA (1 μg) was used to synthesize cDNA with the iScript kit (Bio-Rad, #170-8891) following the manufacturer's protocol. qRT-PCR reactions were set up using SoAdvanced SYBR green (Bio-Rad, #172-5265). Primers used are listed in supplementary material Table S1.

Velocity field generation and analysis

Particle Image Velocimetry (PIV)-type analysis was applied to time-lapse images collected at a single confocal plane parallel to the animal-vegetal axis that passed through the center of the embryo. Three passes using sub-windows of 64, 32 and 16 pixels with an overlap of 50% were used to compute the velocity fields. The region of the image outside of the embryo was masked from the analysis and did not contribute to any of the sub-window matching. Prior to analysis, the contribution of spurious vectors was reduced by time-averaging velocity fields with a boxcar moving average filter of width 2. Three regions were defined for the analysis: a center region and two symmetric side regions. A vector extending from the vegetal-to-animal pole was defined to adjust for different absolute orientations of the embryos. For each of the three flow regions, the overall average magnitude

and average magnitude in the animal pole direction were calculated as a function of time.

Ovary histology and confocal immunofluorescence

Females were anesthetized in Tricaine as described (Westerfield, 1995). Ovaries were dissected and fixed in 4% PFA overnight. Sectioning and hematoxylin & eosin (H&E) staining were performed as in Hartung et al. (2014). Images were acquired using an Axioskop2 microscope and an AxioCam CCD camera (Zeiss).

Anesthetized WT of *dchs1b*^{fh275/fh275} females were squeezed to obtain unfertilized eggs, which were fixed immediately or at 0 and 2 mpa. For β -catenin and γ -tubulin IHC, samples were fixed with 4% PFA and were performed using either anti- β -catenin (C2206, Sigma) or anti- γ -tubulin (T5326, Sigma) antibodies diluted 1:1000. For tubulin IHC, samples were fixed according to Gard (1991) and were performed using anti-acetylated α -tubulin (T6793, Sigma) diluted 1:1000. Alexa Fluor 488 and Alexa Fluor 568 (Invitrogen) secondary antibodies were diluted 1:500. For F-actin labeling, samples were fixed for 4 h at 4°C in 3.7% formaldehyde in Actin stabilizing buffer (ASB) as in Becker and Hart (1999), then staining of oocytes was performed as described in Topczewski and Solnica-Krezel (1999) using 66 nM Rhodamine Phalloidin (R415, Life Technologies) for 1 h at RT. F-actin labeling of polar bodies was performed as described in Dekens et al. (2003) using 33 nM Rhodamine Phalloidin (R415, Life Technologies) overnight at 4°C . All fluorescently labeled samples were mounted in VECTASHIELD with DAPI (H-1200, Vector Laboratories). Maximal z -projections of AcTub immunostaining were thresholded using ImageJ, and the number of objects $\geq 3\text{ }\mu\text{m}^2$ was calculated with the 'Analyze Particles' feature. Images of F-actin-labeled polar bodies were acquired with a Zeiss LSM5 Live DuoScan line-scanning confocal image using a $10\times/0.45$ air objective. All other samples were imaged with a Leica SP2 point-scanning confocal microscope using either the $40\times/1.25$ or $63\times/1.4$ oil-immersion objective.

Pharmacological treatments

Eggs were fertilized *in vitro*, activated and cultured in egg water containing 3 $\mu\text{g/ml}$ of cytochalasin D (Sigma, #C8273), 0.05 μM of nocodazole (Sigma, #M1404) or 1 μM taxol (Sigma, #T7191) in DMSO until desired stages. For live-imaging, embryos treated with 3 $\mu\text{g/ml}$ of cytochalasin D were dechorionated after 8 min and mounted in 0.3% LMA containing 3 $\mu\text{g/ml}$ cytochalasin D on a round #1 coverglass bottom dish. Control embryos were treated with equivalent amounts of DMSO.

Molecular cloning

To generate the *dchs1b-sfGFP* and *dchs1b* intracellular domain constructs, the full-length *dchs1b* ORF or intracellular domain exon was obtained by multi-step PCR and subcloning from zebrafish cDNA prepared by SuperScript III RT (Invitrogen). The full-length *dchs1b* ORF was further fused in frame with a 9aa linker and the *sfGFP* sequences by annealing extend PCR. The intracellular domain sequence spans from amino acid 2398 to amino acid 2756.

Statistical analyses

Statistical analysis was performed using GraphPad Prism 6. Statistical significance was estimated using a two-tailed unpaired Student's *t*-test to compare two populations.

Acknowledgements

We thank Diane Sepich, Margot Williams and other members of the L.S.-K. lab for discussion and comments on the manuscript, and our fish facility staff for excellent animal care. We also thank Carl-Philipp Heisenberg, Benjamin Feldman, Marina Mione and Karuna Sampath for sharing reagents.

Competing interests

The authors declare no competing or financial interests.

Author contributions

N.L.-V., M.M.F., A.J.L., F.L.M., G.D.L. and L.S.-K. conceived and designed the experiments, analyzed and discussed the data, and wrote the manuscript. N.L.-V., M.M.F. and A.J.L. performed the experiments. N.L.-V., J.C., T.M., K.H.,

C.B.M., J.S., A.S., A.E.H., J.D. and A.F.S. contributed reagents, materials and analysis tools.

Funding

This work was supported in part by grants from the National Institutes of Health (NIH) [R01GM55101 to L.S.-K.]; [R01GM089979 to F.L.M.]; Training Program in Developmental Biology [2T32HD007502-16A1] in support of N.L.V.; and [T32-GM007491] in support of M.M.F. Deposited in PMC for release after 12 months.

Supplementary material

Supplementary material available online at
<http://dev.biologists.org/lookup/suppl/doi:10.1242/dev.119800/-DC1>

References

- Adler, P. N., Charlton, J. and Liu, J. (1998). Mutations in the cadherin superfamily member gene dachsous cause a tissue polarity phenotype by altering frizzled signaling. *Development* **125**, 959-968.
- Agius, E., Oelgeschlager, M., Wessely, O., Kemp, C. and De Robertis, E. M. (2000). Endodermal Nodal-related signals and mesoderm induction in Xenopus. *Development* **127**, 1173-1183.
- Alexander, J. and Stainier, D. Y. R. (1999). A molecular pathway leading to endoderm formation in zebrafish. *Curr. Biol.* **9**, 1147-1157.
- Anani, S., Bhat, S., Honma-Yamanaka, N., Krawchuk, D. and Yamanaka, Y. (2014). Initiation of Hippo signaling is linked to polarity rather than to cell position in the pre-implantation mouse embryo. *Development* **141**, 2813-2824.
- Baena-Lopez, L. A., Rodriguez, I. and Baonza, A. (2008). The tumor suppressor genes dachsous and fat modulate different signalling pathways by regulating dally and dally-like. *Proc. Natl. Acad. Sci. USA* **105**, 9645-9650.
- Becker, K. A. and Hart, N. H. (1999). Reorganization of filamentous actin and myosin-II in zebrafish eggs correlates temporally and spatially with cortical granule exocytosis. *J. Cell Sci.* **112**, 97-110.
- Behrndt, M., Salbreux, G., Campinho, P., Hauschild, R., Oswald, F., Roensch, J., Grill, S. W. and Heisenberg, C.-P. (2012). Forces driving epithelial spreading in zebrafish gastrulation. *Science* **338**, 257-260.
- Bertrand, A. T., Ziae, S., Ehret, C., Duchemin, H., Mamchaoui, K., Bigot, A., Mayer, M., Quijano-Roy, S., Desguerre, I., Laine, J. et al. (2014). Cellular microenvironments reveal defective mechanosensing responses and elevated YAP signaling in LMNA-mutated muscle precursors. *J. Cell Sci.* **127**, 2873-2884.
- Brunet, T., Bouclet, A., Ahmadi, P., Mitrossilis, D., Driuez, B., Brunet, A.-C., Henry, L., Serman, F., Béalle, G., Ménager, C. et al. (2013). Evolutionary conservation of early mesoderm specification by meiotransduction in Bilateria. *Nat. Commun.* **4**, 2821.
- Campinho, P., Behrndt, M., Ranft, J., Risler, T., Minc, N. and Heisenberg, C.-P. (2013). Tension-oriented cell divisions limit anisotropic tissue tension in epithelial spreading during zebrafish epiboly. *Nat. Cell Biol.* **15**, 1405-1414.
- Cappello, S., Gray, M. J., Badouel, C., Lange, S., Einsiedler, M., Srour, M., Chitayat, D., Hamdan, F. F., Jenkins, Z. A., Morgan, T. et al. (2013). Mutations in genes encoding the cadherin receptor-ligand pair DCHS1 and FAT4 disrupt cerebral cortical development. *Nat. Genet.* **45**, 1300-1308.
- Carvalho, L. and Heisenberg, C.-P. (2010). The yolk syncytial layer in early zebrafish development. *Trends Cell Biol.* **20**, 586-592.
- Carvalho, L., Stuhmer, J., Bois, J. S., Kalaidzidis, Y., Lecaudey, V. and Heisenberg, C.-P. (2009). Control of convergent yolk syncytial layer nuclear movement in zebrafish. *Development* **136**, 1305-1315.
- Casal, J., Struhl, G. and Lawrence, P. A. (2002). Developmental compartments and planar polarity in Drosophila. *Curr. Biol.* **12**, 1189-1198.
- Casal, J., Lawrence, P. A. and Struhl, G. (2006). Two separate molecular systems, Dachsous/Fat and Starry night/Frizzled, act independently to confer planar cell polarity. *Development* **133**, 4561-4572.
- Chang, Y.-F., Imam, J. S. and Wilkinson, M. F. (2007). The nonsense-mediated decay RNA surveillance pathway. *Annu. Rev. Biochem.* **76**, 51-74.
- Chen, S. and Kimelman, D. (2000). The role of the yolk syncytial layer in germ layer patterning in zebrafish. *Development* **127**, 4681-4689.
- Chen, Y. and Schier, A. F. (2001). The zebrafish Nodal signal Squint functions as a morphogen. *Nature* **411**, 607-610.
- Cho, E. and Irvine, K. D. (2004). Action of fat, four-jointed, dachsous and dachs in distal-to-proximal wing signaling. *Development* **131**, 4489-4500.
- Cho, E., Feng, Y., Rauskolb, C., Maitra, S., Fehon, R. and Irvine, K. D. (2006). Delineation of a Fat tumor suppressor pathway. *Nat. Genet.* **38**, 1142-1150.
- Ciruna, B., Jenny, A., Lee, D., Mlodzik, M. and Schier, A. F. (2006). Planar cell polarity signalling couples cell division and morphogenesis during neurulation. *Nature* **439**, 220-224.
- Clark, H. F., Breitnrup, D., Schneitz, K., Bieber, A., Goodman, C. and Noll, M. (1995). Dachsous encodes a member of the cadherin superfamily that controls imaginal disc morphogenesis in Drosophila. *Genes Dev.* **9**, 1530-1542.
- Cooper, J. A. (1987). Effects of cytochalasin and phalloidin on actin. *J. Cell Biol.* **105**, 1473-1478.
- D'Amico, L. A. and Cooper, M. S. (2001). Morphogenetic domains in the yolk syncytial layer of axiating zebrafish embryos. *Dev. Dyn.* **222**, 611-624.
- Dekens, M. P. S., Pelegri, F. J., Maischein, H.-M. and Nüsslein-Volhard, C. (2003). The maternal-effect gene futile cycle is essential for pronuclear congression and mitotic spindle assembly in the zebrafish zygote. *Development* **130**, 3907-3916.
- Donoughe, S. and DiNardo, S. (2011). dachsous and frizzled contribute separately to planar polarity in the Drosophila ventral epidermis. *Development* **138**, 2751-2759.
- Dosch, R., Wagner, D. S., Mintzer, K. A., Runke, G., Wiemelt, A. P. and Mullins, M. C. (2004). Maternal control of vertebrate development before the midblastula transition: mutants from the zebrafish I. *Dev. Cell* **6**, 771-780.
- Draper, B. W., McCallum, C. M., Stout, J. L., Slade, A. J. and Moens, C. B. (2004). A high-throughput method for identifying N-ethyl-N-nitrosourea (ENU)-induced point mutations in zebrafish. *Methods Cell Biol.* **77**, 91-112.
- Dubrulle, J., Jordan, B. M., Akhmetova, L., Farrell, J. A., Kim, S. H., Solnica-Krezel, L. and Schier, A. F. (2015) Response to Nodal morphogen gradient is determined by the kinetics of target gene induction. *Elife* **4**, e05042.
- Engleka, M. J., Craig, E. J. and Kessler, D. S. (2001). VegT activation of Sox17 at the midblastula transition alters the response to nodal signals in the vegetal endoderm domain. *Dev. Biol.* **237**, 159-172.
- Erter, C. E., Solnica-Krezel, L. and Wright, C. V. E. (1998). Zebrafish nodal-related 2 encodes an early mesendodermal inducer signaling from the extraembryonic yolk syncytial layer. *Dev. Biol.* **204**, 361-372.
- Fekany, K., Yamanaka, Y., Leung, T., Sirotkin, H. I., Topczewski, J., Gates, M. A., Hibi, M., Renucci, A., Stemple, D., Radbill, A. et al. (1999). The zebrafish bozozok locus encodes Dharma, a homeodomain protein essential for induction of gastrula organizer and dorsoanterior embryonic structures. *Development* **126**, 1427-1438.
- Feldman, B., Gates, M. A., Egan, E. S., Dougan, S. T., Rennebeck, G., Sirotkin, H. I., Schier, A. F. and Talbot, W. S. (1998). Zebrafish organizer development and germ-layer formation require nodal-related signals. *Nature* **395**, 181-185.
- Fernandez, J., Valladares, M., Fuentes, R. and Ubilla, A. (2006). Reorganization of cytoplasm in the zebrafish oocyte and egg during early steps of ooplasmic segregation. *Dev. Dyn.* **235**, 656-671.
- Fuentes, R. and Fernandez, J. (2010). Ooplasmic segregation in the zebrafish zygote and early embryo: pattern of ooplasmic movements and transport pathways. *Dev. Dyn.* **239**, 2172-2189.
- Gard, D. L. (1991). Organization, nucleation, and acetylation of microtubules in *Xenopus laevis* oocytes: a study by confocal immunofluorescence microscopy. *Dev. Biol.* **143**, 346-362.
- Ge, X., Grotjahn, D., Welch, E., Lyman-Gingerich, J., Holguin, C., Dimitrova, E., Abrams, E. W., Gupta, T., Marlow, F. L., Yabe, T. et al. (2014). Hecate/Grip2a acts to reorganize the cytoskeleton in the symmetry-breaking event of embryonic axis induction. *PLoS Genet.* **10**, e1004422.
- Goodrich, L. V. and Strutt, D. (2011). Principles of planar polarity in animal development. *Development* **138**, 1877-1892.
- Gore, A. V. and Sampath, K. (2002). Localization of transcripts of the zebrafish morphogen Squint is dependent on egg activation and the microtubule cytoskeleton. *Mech. Dev.* **112**, 153-156.
- Gritsman, K., Talbot, W. S. and Schier, A. F. (2000). Nodal signaling patterns the organizer. *Development* **127**, 921-932.
- Hart, N. H. (1990). Fertilization in teleost fishes: mechanisms of sperm-egg interactions. *Int. Rev. Cytol.* **121**, 1-66.
- Hart, N. H. and Fluck, R. A. (1996). Cytoskeleton in teleost eggs and early embryos: contributions to cytoarchitecture and motile events. *Curr. Top. Dev. Biol.* **31**, 343-381.
- Hartung, O., Forbes, M. M. and Marlow, F. L. (2014). Zebrafish vasa is required for germ-cell differentiation and maintenance. *Mol. Reprod. Dev.* **81**, 946-961.
- Harumoto, T., Ito, M., Shimada, Y., Kobayashi, T. J., Ueda, H. R., Lu, B. and Uemura, T. (2010). Atypical cadherins Dachsous and Fat control dynamics of noncentrosomal microtubules in planar cell polarity. *Dev. Cell* **19**, 389-401.
- Heallen, T., Zhang, M., Wang, J., Bonilla-Claudio, M., Klysik, E., Johnson, R. L. and Martin, J. F. (2011). Hippo pathway inhibits Wnt signaling to restrain cardiomyocyte proliferation and heart size. *Science* **332**, 458-461.
- Heidemann, S. R., Zieve, G. W. and McIntosh, J. R. (1980). Evidence for microtubule subunit addition to the distal end of mitotic structures in vitro. *J. Cell Biol.* **87**, 152-159.
- Heisenberg, C.-P., Tada, M., Rauch, G.-J., Saúde, L., Concha, M. L., Geisler, R., Stemple, D. L., Smith, J. C. and Wilson, S. W. (2000). Silberblick/Wnt11 mediates convergent extension movements during zebrafish gastrulation. *Nature* **405**, 76-81.
- Hirate, Y., Hirahara, S., Inoue, K.-I., Suzuki, A., Alarcon, V. B., Akimoto, K., Hirai, T., Hara, T., Adachi, M., Chida, K. et al. (2013). Polarity-dependent distribution of angiominotin localizes Hippo signaling in preimplantation embryos. *Curr. Biol.* **23**, 1181-1194.
- Hong, S.-K., Jang, M. K., Brown, J. L., McBride, A. A. and Feldman, B. (2011). Embryonic mesoderm and endoderm induction requires the actions of non-embryonic Nodal-related ligands and Mxtx2. *Development* **138**, 787-795.

- Houston, D. W.** (2013). Regulation of cell polarity and RNA localization in vertebrate oocytes. *Int. Rev. Cell Mol. Biol.* **306**, 127-185.
- Hudson, C., Clements, D., Friday, R. V., Stott, D. and Woodland, H. R.** (1997). Xsox17alpha and -beta mediate endoderm formation in *Xenopus*. *Cell* **91**, 397-405.
- Imajo, M., Miyatake, K., Iimura, A., Miyamoto, A. and Nishida, E.** (2012). A molecular mechanism that links Hippo signalling to the inhibition of Wnt/beta-catenin signalling. *EMBO J.* **31**, 1109-1122.
- Ishikawa, H. O., Takeuchi, H., Haltiwanger, R. S. and Irvine, K. D.** (2008). Four-jointed is a Golgi kinase that phosphorylates a subset of cadherin domains. *Science* **321**, 401-404.
- Ishiuchi, T., Misaki, K., Yonemura, S., Takeichi, M. and Tanoue, T.** (2009). Mammalian Fat and Dachsous cadherins regulate apical membrane organization in the embryonic cerebral cortex. *J. Cell Biol.* **185**, 959-967.
- Ivanenkov, V. V., Minin, A. A., Meshcheryakov, V. N. and Martynova, L. E.** (1987). The effect of local cortical microfilament disorganization on ooplasmic segregation in the loach (*Misgurnus fossilis*) egg. *Cell Differ.* **22**, 19-28.
- Jessen, J. R., Topczewski, J., Bingham, S., Sepich, D. S., Marlow, F., Chandrasekhar, A. and Solnica-Krezel, L.** (2002). Zebrafish trilobite identifies new roles for Strabismus in gastrulation and neuronal movements. *Nat. Cell Biol.* **4**, 610-615.
- Jesuthasan, S. and Strähle, U.** (1997). Dynamic microtubules and specification of the zebrafish embryonic axis. *Curr. Biol.* **7**, 31-42.
- Jones, C. M., Kuehn, M. R., Hogan, B. L., Smith, J. C. and Wright, C. V.** (1995). Nodal-related signals induce axial mesoderm and dorsalize mesoderm during gastrulation. *Development* **121**, 3651-3662.
- Kane, D. A. and Kimmel, C. B.** (1993). The zebrafish midblastula transition. *Development* **119**, 447-456.
- Kelly, C., Chin, A. J., Leatherman, J. L., Kozlowski, D. J. and Weinberg, E. S.** (2000). Maternally controlled (beta)-catenin-mediated signalling is required for organizer formation in the zebrafish. *Development* **127**, 3899-3911.
- Kimmel, C. B., Ballard, W. W., Kimmel, S. R., Ullmann, B. and Schilling, T. F.** (1995). Stages of embryonic development of the zebrafish. *Dev. Dyn.* **203**, 253-310.
- Kono, K., Tamashiro, D. A. A. and Alarcon, V. B.** (2014). Inhibition of RHO-ROCK signaling enhances ICM and suppresses TE characteristics through activation of Hippo signaling in the mouse blastocyst. *Dev. Biol.* **394**, 142-155.
- Kosaka, K., Kawakami, K., Sakamoto, H. and Inoue, K.** (2007). Spatiotemporal localization of germ plasm RNAs during zebrafish oogenesis. *Mech. Dev.* **124**, 279-289.
- Lachnit, M., Kur, E. and Driever, W.** (2008). Alterations of the cytoskeleton in all three embryonic lineages contribute to the epiboly defect of Pou5f1/Oct4 deficient MZspg zebrafish embryos. *Dev. Biol.* **315**, 1-17.
- Le Pabic, P., Ng, C. and Schilling, T. F.** (2014). Fat-Dachsous signaling coordinates cartilage differentiation and polarity during craniofacial development. *PLoS Genet.* **10**, e1004726.
- Leung, C. F., Webb, S. E. and Miller, A. L.** (2000). On the mechanism of ooplasmic segregation in single-cell zebrafish embryos. *Dev. Growth Differ.* **42**, 29-40.
- Low, B. C., Pan, C. Q., Shivasankar, G. V., Bershadsky, A., Sudol, M. and Sheetz, M.** (2014). YAP/TAZ as mechanosensors and mechanotransducers in regulating organ size and tumor growth. *FEBS Lett.* **588**, 2663-2670.
- Lu, F.-I., Thisse, C. and Thisse, B.** (2011). Identification and mechanism of regulation of the zebrafish dorsal determinant. *Proc. Natl. Acad. Sci. USA* **108**, 15876-15880.
- Lucas, E. P., Khanal, I., Gaspar, P., Fletcher, G. C., Polesello, C., Tapon, N. and Thompson, B. J.** (2013). The Hippo pathway polarizes the actin cytoskeleton during collective migration of Drosophila border cells. *J. Cell Biol.* **201**, 875-885.
- Ma, D., Yang, C.-H., McNeill, H., Simon, M. A. and Axelrod, J. D.** (2003). Fidelity in planar cell polarity signalling. *Nature* **421**, 543-547.
- Mao, Y., Rauskolb, C., Cho, E., Hu, W.-L., Hayter, H., Minihan, G., Katz, F. N. and Irvine, K. D.** (2006). Dachs: an unconventional myosin that functions downstream of Fat to regulate growth, affinity and gene expression in Drosophila. *Development* **133**, 2539-2551.
- Mao, Y., Mulvaney, J., Zakaria, S., Yu, T., Morgan, K. M., Allen, S., Basson, M. A., Francis-West, P. and Irvine, K. D.** (2011). Characterization of a Dchs1 mutant mouse reveals requirements for Dchs1-Fat4 signaling during mammalian development. *Development* **138**, 947-957.
- Marlow, F., Zwartkruis, F., Malicki, J., Neuhauss, S. C. F., Abbas, L., Weaver, M., Driever, W. and Solnica-Krezel, L.** (1998). Functional interactions of genes mediating convergent extension, knypek and trilobite, during the partitioning of the eye primordium in zebrafish. *Dev. Biol.* **203**, 382-399.
- Matakatsu, H. and Blair, S. S.** (2004). Interactions between Fat and Dachsous and the regulation of planar cell polarity in the Drosophila wing. *Development* **131**, 3785-3794.
- Matis, M., Russler-Germain, D. A., Hu, Q., Tomlin, C. J. and Axelrod, J. D.** (2014). Microtubules provide directional information for core PCP function. *Elife* **3**, e02893.
- Mei, W., Lee, K. W., Marlow, F. L., Miller, A. L. and Mullins, M. C.** (2009). hnRNP I is required to generate the Ca²⁺ signal that causes egg activation in zebrafish. *Development* **136**, 3007-3017.
- Mizuno, T., Yamaha, E., Kuroiwa, A. and Takeda, H.** (1999). Removal of vegetal yolk causes dorsal deficiencies and impairs dorsal-inducing ability of the yolk cell in zebrafish. *Mech. Dev.* **81**, 51-63.
- Muller, P., Rogers, K. W., Yu, S. R., Brand, M. and Schier, A. F.** (2013). Morphogen transport. *Development* **140**, 1621-1638.
- Nojima, H., Shimizu, T., Kim, C.-H., Yabe, T., Bae, Y.-K., Muraoka, O., Hirata, T., Chitnis, A., Hirano, T. and Hibi, M.** (2004). Genetic evidence for involvement of maternally derived Wnt canonical signaling in dorsal determination in zebrafish. *Mech. Dev.* **121**, 371-386.
- Nojima, H., Rothamel, S., Shimizu, T., Kim, C.-H., Yonemura, S., Marlow, F. L. and Hibi, M.** (2010). Syntabulin, a motor protein linker, controls dorsal determination. *Development* **137**, 923-933.
- Prasad, A. K. and Jensen, K.** (1995). Scheimpflug stereocamera for particle image velocimetry in liquid flows. *Appl. Opt.* **34**, 7092-7099.
- Rawls, A. S., Guinto, J. B. and Wolff, T.** (2002). The cadherins fat and dachsous regulate dorsal/ventral signaling in the Drosophila eye. *Curr. Biol.* **12**, 1021-1026.
- Rodaway, A., Takeda, H., Koshida, S., Broadbent, J., Price, B., Smith, J. C., Patient, R. and Holder, N.** (1999). Induction of the mesendoderm in the zebrafish germ ring by yolk cell-derived TGF-beta family signals and discrimination of mesoderm and endoderm by FGF. *Development* **126**, 3067-3078.
- Saka, Y., Hagemann, A. I., Piepenburg, O. and Smith, J. C.** (2007). Nuclear accumulation of Smad complexes occurs only after the midblastula transition in *Xenopus*. *Development* **134**, 4209-4218.
- Sampath, K., Rubinstein, A. L., Cheng, A. M., Liang, J. O., Fekany, K., Solnica-Krezel, L., Korzh, V., Halpern, M. E. and Wright, C. V.** (1998). Induction of the zebrafish ventral brain and floorplate requires cyclops/nodal signalling. *Nature* **395**, 185-189.
- Schier, A. F. and Shen, M. M.** (2000). Nodal signalling in vertebrate development. *Nature* **403**, 385-389.
- Schlüwa, M.** (1982). Action of cytochalasin D on cytoskeletal networks. *J. Cell Biol.* **92**, 79-91.
- Schulte-Merker, S., Ho, R. K., Herrmann, B. G. and Nüsslein-Volhard, C.** (1992). The protein product of the zebrafish homologue of the mouse T gene is expressed in nuclei of the germ ring and the notochord of the early embryo. *Development* **116**, 1021-1032.
- Schulte-Merker, S., van Eeden, F. J., Halpern, M. E., Kimmel, C. B. and Nüsslein-Volhard, C.** (1994). no tail (ntl) is the zebrafish homologue of the mouse T (Brachyury) gene. *Development* **120**, 1009-1015.
- Schulte-Merker, S., Lee, K. J., McMahon, A. P. and Hammerschmidt, M.** (1997). The zebrafish organizer requires chordino. *Nature* **387**, 862-863.
- Shao, M., Lin, Y., Liu, Z., Zhang, Y., Wang, L., Liu, C. and Zhang, H.** (2012). GSK-3 activity is critical for the orientation of the cortical microtubules and the dorsoventral axis determination in zebrafish embryos. *PLoS ONE* **7**, e36655.
- Shimizu, T., Yamanaka, Y., Ryu, S.-L., Hashimoto, H., Yabe, T., Hirata, T., Bae, Y.-K., Hibi, M. and Hirano, T.** (2000). Cooperative roles of Bozozok/Dharma and Nodal-related proteins in the formation of the dorsal organizer in zebrafish. *Mech. Dev.* **91**, 293-303.
- Simon, M. A., Xu, A., Ishikawa, H. O. and Irvine, K. D.** (2010). Modulation of fat: dachsous binding by the cadherin domain kinase four-jointed. *Curr. Biol.* **20**, 811-817.
- Sirotnik, H. I., Dougan, S. T., Schier, A. F. and Talbot, W. S.** (2000). bozozok and squint act in parallel to specify dorsal mesoderm and anterior neuroectoderm in zebrafish. *Development* **127**, 2583-2592.
- Solnica-Krezel, L.** (2005). Conserved patterns of cell movements during vertebrate gastrulation. *Curr. Biol.* **15**, R213-R228.
- Solnica-Krezel, L. and Driever, W.** (1994). Microtubule arrays of the zebrafish yolk cell: organization and function during epiboly. *Development* **120**, 2443-2455.
- Solnica-Krezel, L. and Driever, W.** (2001). The role of the homeodomain protein Bozozok in zebrafish axis formation. *Int. J. Dev. Biol.* **45**, 299-310.
- Stern, C. D.** (1992). Mesoderm induction and development of the embryonic axis in amniotes. *Trends Genet.* **8**, 158-163.
- Strutt, H. and Strutt, D.** (2002). Planar polarity: photoreceptors on a high fat diet. *Curr. Biol.* **12**, R384-R385.
- Takeichi, M.** (1995). Morphogenetic roles of classic cadherins. *Curr. Opin. Cell Biol.* **7**, 619-627.
- Talevi, R., Gualtieri, R., Tartaglione, G. and Fortunato, A.** (1997). Heterogeneity of the zona pellucida carbohydrate distribution in human oocytes failing to fertilize in vitro. *Hum. Reprod.* **12**, 2773-2780.
- Taylor, J. S., Braasch, I., Frickey, T., Meyer, A. and Van de Peer, Y.** (2003). Genome duplication, a trait shared by 22,000 species of ray-finned fish. *Genome Res.* **13**, 382-390.
- Thisse, C. and Thisse, B.** (2008). High-resolution *in situ* hybridization to whole-mount zebrafish embryos. *Nat. Protoc.* **3**, 59-69.
- Topczewski, J. and Solnica-Krezel, L.** (1999). Cytoskeletal dynamics of the zebrafish embryo. *Methods Cell Biol.* **59**, 205-226.
- Topczewski, J., Sepich, D. S., Myers, D. C., Walker, C., Amores, A., Lele, Z., Hammerschmidt, M., Postlethwait, J. and Solnica-Krezel, L.** (2001). The zebrafish glycan knypek controls cell polarity during gastrulation movements of convergent extension. *Dev. Cell* **1**, 251-264.

- Tran, L. D., Hino, H., Quach, H., Lim, S., Shindo, A., Mimori-Kiyosue, Y., Mione, M., Ueno, N., Winkler, C., Hibi, M. et al. (2012). Dynamic microtubules at the vegetal cortex predict the embryonic axis in zebrafish. *Development* **139**, 3644-3652.
- Tsaadon, A., Eliyahu, E., Shraizent, N. and Shalgi, R. (2006). When a sperm meets an egg: block to polyspermy. *Mol. Cell. Endocrinol.* **252**, 107-114.
- Varelas, X., Miller, B. W., Sopko, R., Song, S., Gregorief, A., Fellouse, F. A., Sakuma, R., Pawson, T., Hunziker, W., McNeill, H. et al. (2010). The Hippo pathway regulates Wnt/beta-catenin signaling. *Dev. Cell* **18**, 579-591.
- Wallace, R. A. and Selman, K. (1990). Ultrastructural aspects of oogenesis and oocyte growth in fish and amphibians. *J. Electron Microsc. Tech.* **16**, 175-201.
- Westerfield, M. (1995). *The Zebrafish Book*. Eugene: University of Oregon Press.
- Wienholds, E. and Plasterk, R. H. A. (2004). Target-selected gene inactivation in zebrafish. *Methods Cell Biol.* **77**, 69-90.
- Wolenski, J. S. and Hart, N. H. (1988). Effects of cytochalasins B and D on the fertilization of zebrafish (*Brachydanio*) eggs. *J. Exp. Zool.* **246**, 202-215.
- Wong, J. L. and Wessel, G. M. (2006). Rendezvin: an essential gene encoding independent, differentially secreted egg proteins that organize the fertilization envelope proteome after self-association. *Mol. Biol. Cell* **17**, 5241-5252.
- Yamanaka, Y., Mizuno, T., Sasai, Y., Kishi, M., Takeda, H., Kim, C.-H., Hibi, M. and Hirano, T. (1998). A novel homeobox gene, dharma, can induce the organizer in a non-cell-autonomous manner. *Genes Dev.* **12**, 2345-2353.
- Yang, C.-H., Axelrod, J. D. and Simon, M. A. (2002). Regulation of Frizzled by fat-like cadherins during planar polarity signaling in the *Drosophila* compound eye. *Cell* **108**, 675-688.
- Yin, C., Kiskowski, M., Pouille, P.-A., Farge, E. and Solnica-Krezel, L. (2008). Cooperation of polarized cell intercalations drives convergence and extension of presomitic mesoderm during zebrafish gastrulation. *J. Cell Biol.* **180**, 221-232.
- Zakaria, S., Mao, Y., Kuta, A., Ferreira de Sousa, C., Gaufo, G. O., McNeill, H., Hindges, R., Guthrie, S., Irvine, K. D. and Francis-West, P. H. (2014). Regulation of neuronal migration by Dchs1-Fat4 planar cell polarity. *Curr. Biol.* **24**, 1620-1627.

Supplementary Material

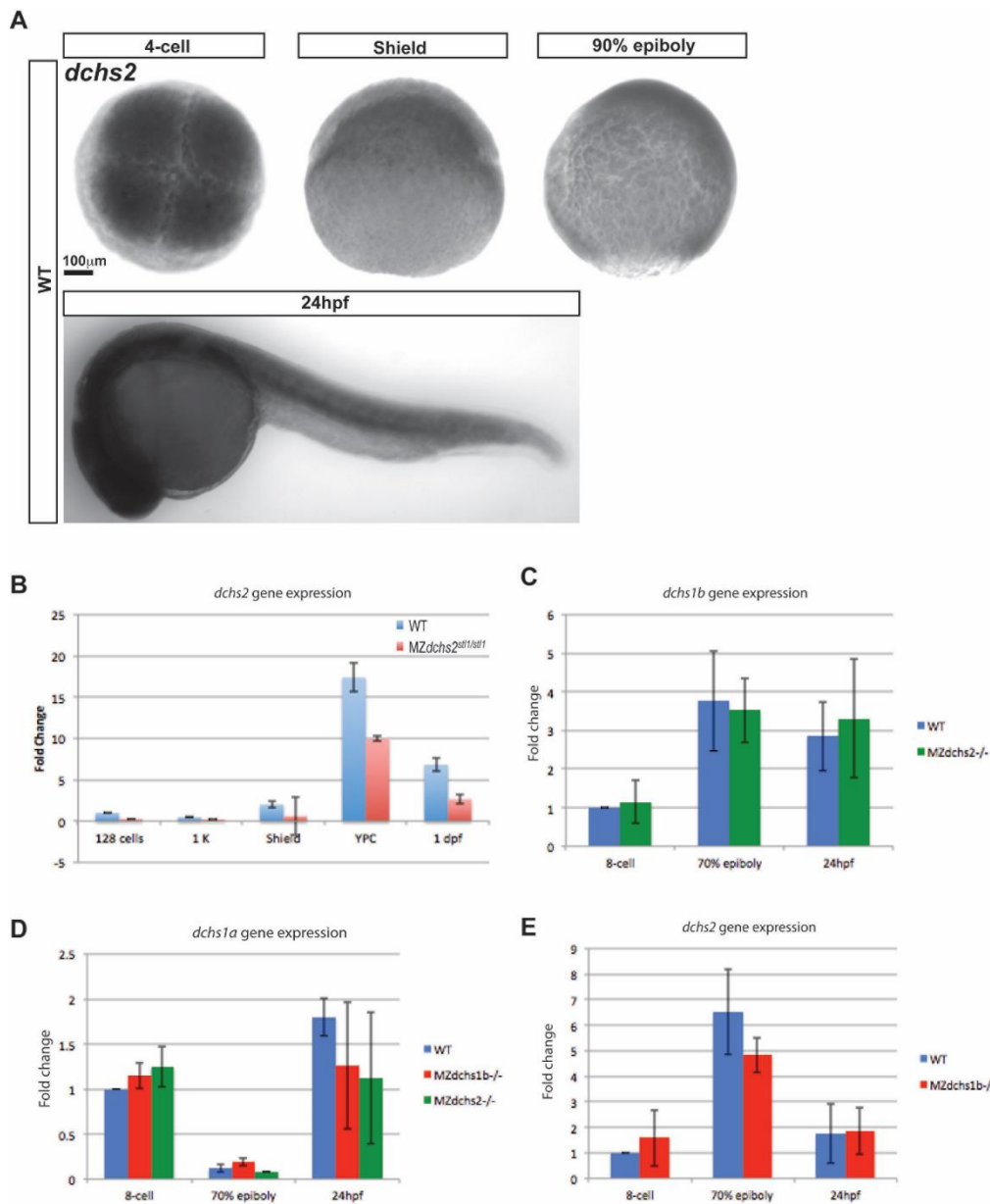
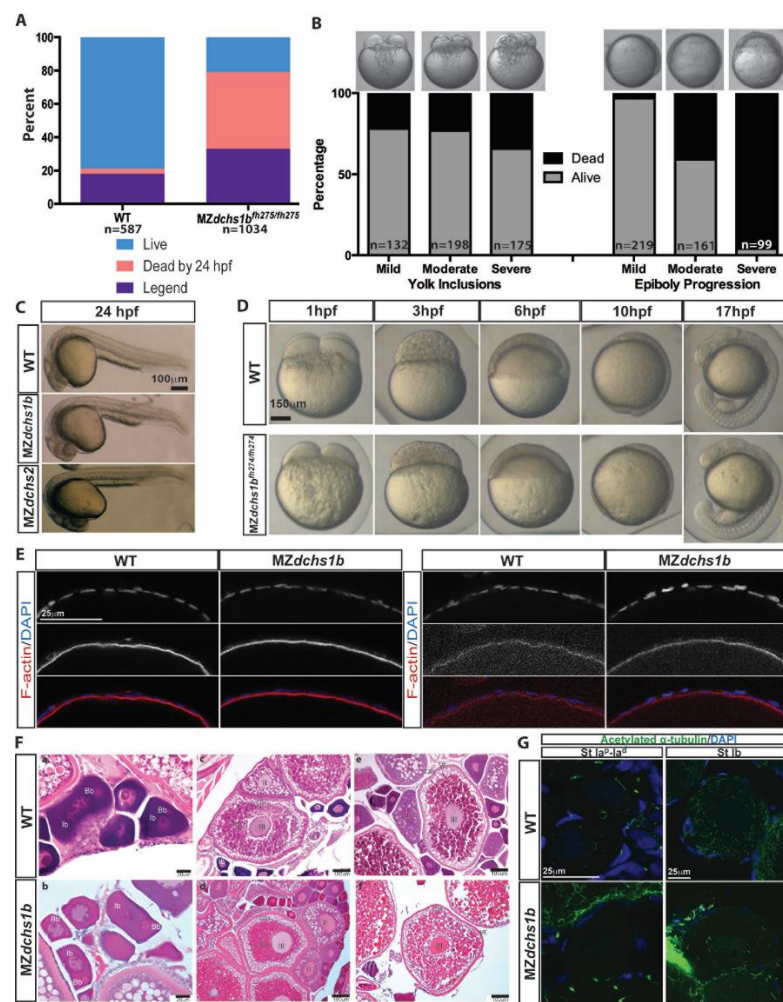


Figure S1 *dchs* expression in zebrafish

- Whole-mount *in situ* hybridization of *dchs2* in WT embryos at 4-cell (1 hpf), shield (6 hpf), 90% epiboly (9 hpf), and 24 hpf stages.
- Quantitative RT-PCR analysis of *dchs2* expression levels in MZdchs2^{stl1/stl1} mutants relative to WT embryos at maternal and zygotic stages.
- Relative expression by qRT-PCR of *dchs1b* in WT and MZdchs1b^{stl1/stl1} embryos.
- Relative expression by qRT-PCR of *dchs1a* in WT, MZdchs1b^{fh275/fh275}, and MZdchs1b^{stl1/stl1} embryos.
- Relative expression by qRT-PCR of *dchs2* in WT and MZdchs1b^{fh275/fh275} embryos.

**Figure S2. Survival, morphology, and histology of WT and *dchs* mutants**

- Survival and fertility for WT (n=587) and MZdchs1b^{fh275/fh275} (n= 1034) mutant embryos.
- Survival of MZdchs1b^{fh275/fh275} embryos based on severity of yolk inclusions and delayed epiboly phenotypes.
- Morphology of WT, MZdchs1b^{fh275/fh275}, and MZdchs1b^{stl1/stl1} embryos at 24 hpf.
- Bright field images of WT and MZdchs1b^{fh275/fh274} time matched embryos at 1, 3, 6, 10, and 17 hpf.
- Rhodamine phalloidin labels actin filaments in the cortical ooplasm and in the follicle cell layer. β -catenin localizes to the oocyte cortex or membrane in stage II oocytes of WT and *dchs1b* mutants.
- Hematoxylin and Eosin (H&E) stained ovary sections of WT and maternal *dachsous* mutant ovaries reveal a normal composition of oocytes. The primary oocytes of WT and *Mdchs* mutant ovaries are polarized as indicated by the presence of the Balbiani body (Bb) in stage Ib oocytes. Cortical granules begin to accumulate in stage II (II) oocytes of WT and *Mdchs* mutants and localize to the cortex in stage III (III) oocytes, which are distinguishable by the presence of yolk granules (Ygs). The structure of the vitelline envelope (VE) surrounding the oocyte is indistinguishable between WT and mutants. Images are representative of oocytes from 3 WT and 3 mutant females examined.
- WT and *dchs1b* mutant oocytes stained with an antibody against acetylated α -tubulin.

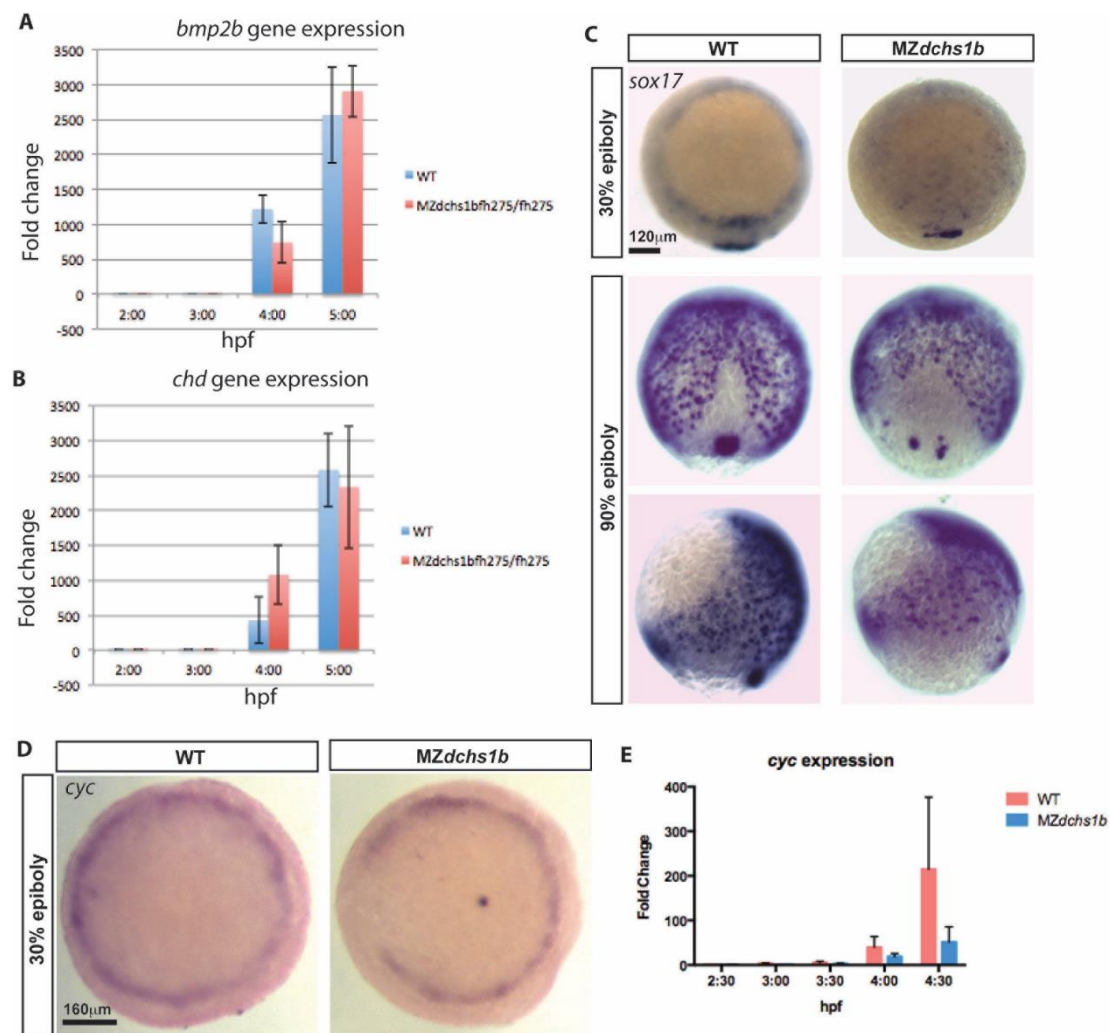


Figure S3. Levels and patterns of zygotic gene expression.

- Expression of zygotic gene *bmp2b* in WT and MZdchs1b embryos during MBT by qRT-PCR.
- Expression of zygotic gene *chd* in WT and MZdchs1b embryos during MBT by qRT-PCR.
- Expression of *sox17* revealed by WISH in stage matched WT and MZdchs1b embryos at 30% and 90% epiboly. Animal pole view for 30% epiboly embryos. Dorsal and later views for 90% epiboly embryos.
- cyc* WISH of stage matched WT and MZdchs1b embryos; animal pole view.
- Quantitative RT-PCR of *cyc* for time matched WT and MZdchs1b embryos during MBT.

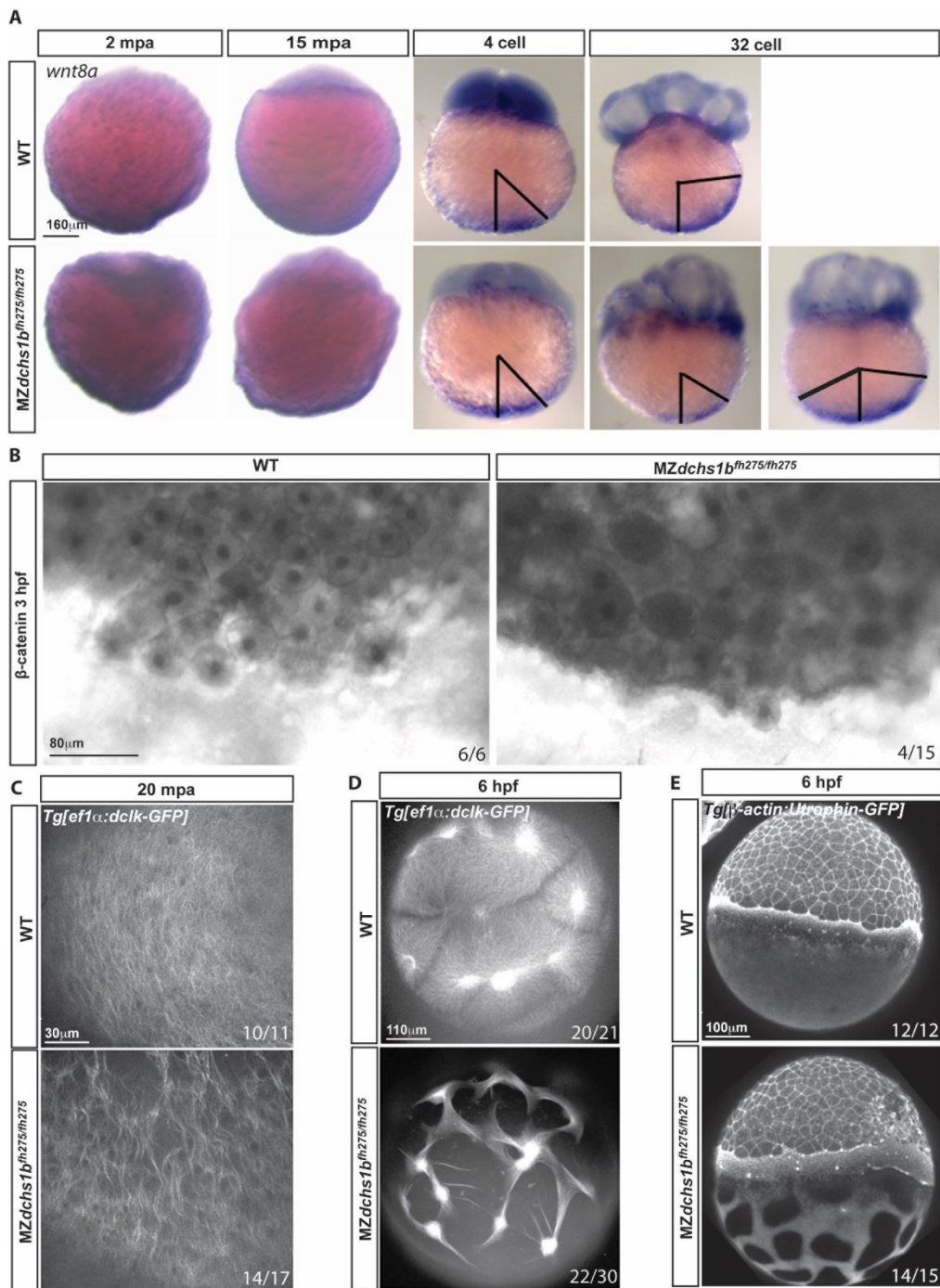


Figure S4. *wnt8a* transport and the cytoskeleton.

- wnt8a* transcripts detected by WISH in WT and MZdchs1b^{fh275/fh275} embryos at 2 mpa, 15 mpa, 4 and 32 cell stages. Representative patterns of *wnt8a* RNA expression domain in MZdchs1b^{fh275/fh275} embryos at 32-cell stage. Black bars mark the angle of the edge of the *wnt8a* RNA expression domain from the vegetal pole.
- β-catenin labeling in 3 hpf WT and MZdchs1b^{fh275/fh275} embryos.
- Max z-projection of parallel array microtubule at 20 mpa in WT and MZdchs1b^{fh275/fh275} embryos.
- Max z-projection of vegetal pole microtubule at 6 hpf in WT and MZdchs1b^{fh275/fh275} embryos.
- Max z-projection of lateral view actin at 6 hpf in WT and MZdchs1b^{fh275/fh275} embryos.

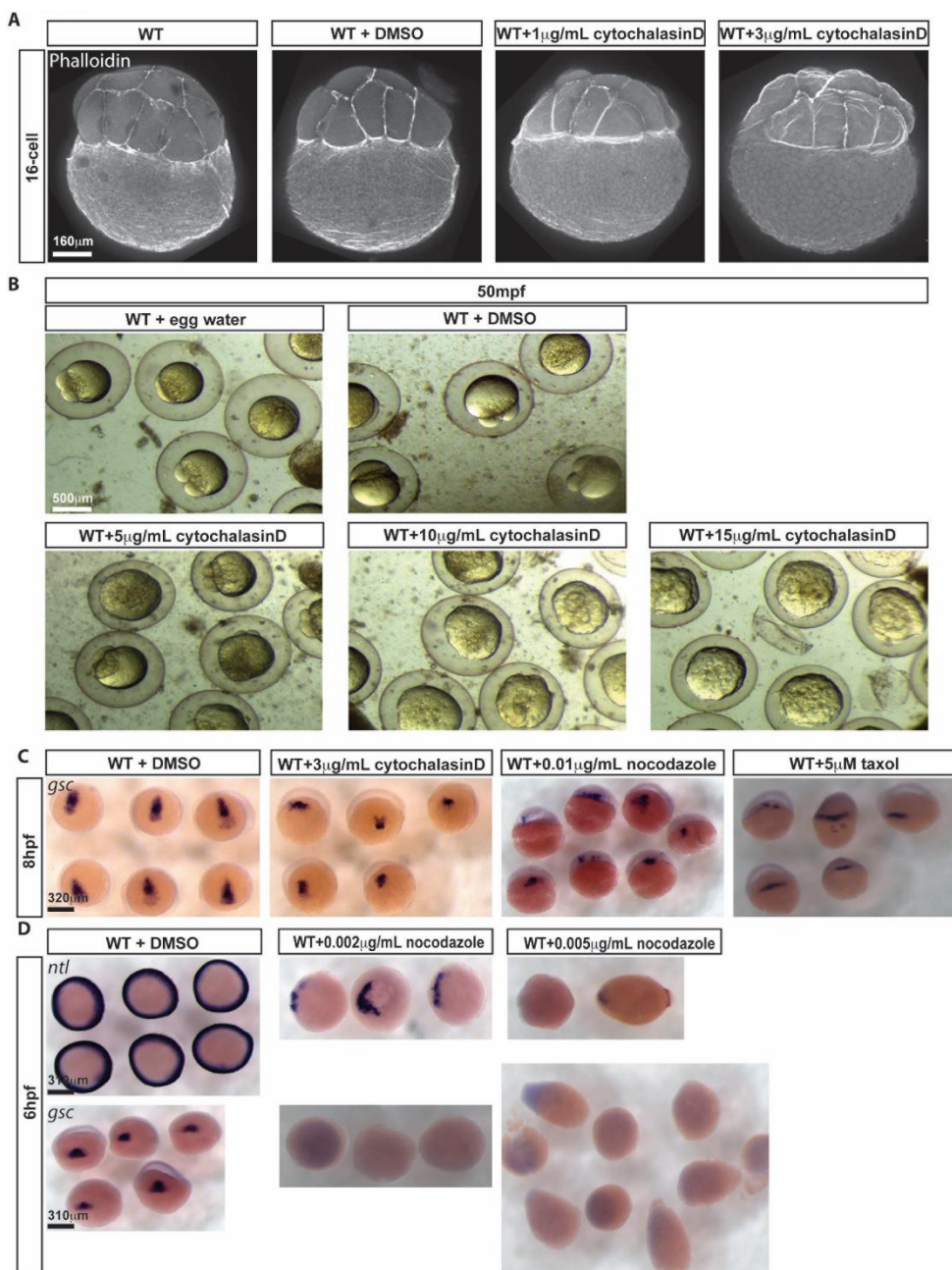


Figure S5. WT embryos treated with cytoskeleton altering agents.

- A. Phalloidin labeling of F-actin at 16-cell stage for WT, WT treated with DMSO, WT treated with 1 μ g/mL cytochalasinD, and WT treated with 3 μ g/mL cytochalasinD from activation.
- B. Bright field images of WT *in vitro* fertilized embryos in egg water, DMSO, 5 μ g/mL cytochalasinD, 10 μ g/mL cytochalasinD, and 15 μ g/mL cytochalasinD from activation at 50mpf.
- C. *gsc* transcripts revealed by WISH in WT embryos treated at 1 hpf with DMSO, 3 μ g/mL cytochalasinD, 0.01 μ g/mL nocodazole, and 5 μ M taxol at 8 hpf; dorsal view.
- D. *ntl* and *gsc* transcripts revealed by WISH in WT embryos treated at 1 hpf with DMSO, 0.002 μ g/mL nocodazole, and 0.005 μ g/mL nocodazole; 6 hpf animal pole view.



Movie S1. Chorion expansion in WT and *MZdchs1b^{fh275/fh275}* mutants.

Time-lapse imaging of WT and *MZdchs1b^{fh275/fh275}* mutants beginning at 40 seconds post activation with interval of 10 seconds for 4 minutes.



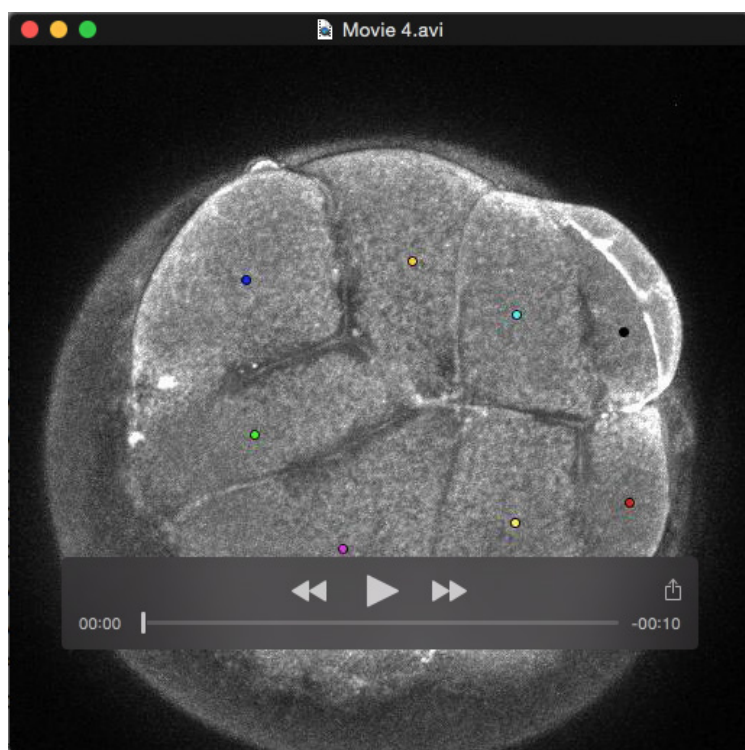
Movie S2. Representative of PIV analysis of WT embryo.

Time-lapse imaging of WT embryo beginning at 8 mpf with interval of 1 minute for 45 minutes. PIV analysis overlay bright field imaging. Red->animal pole ward. Blue->vegetal pole ward.



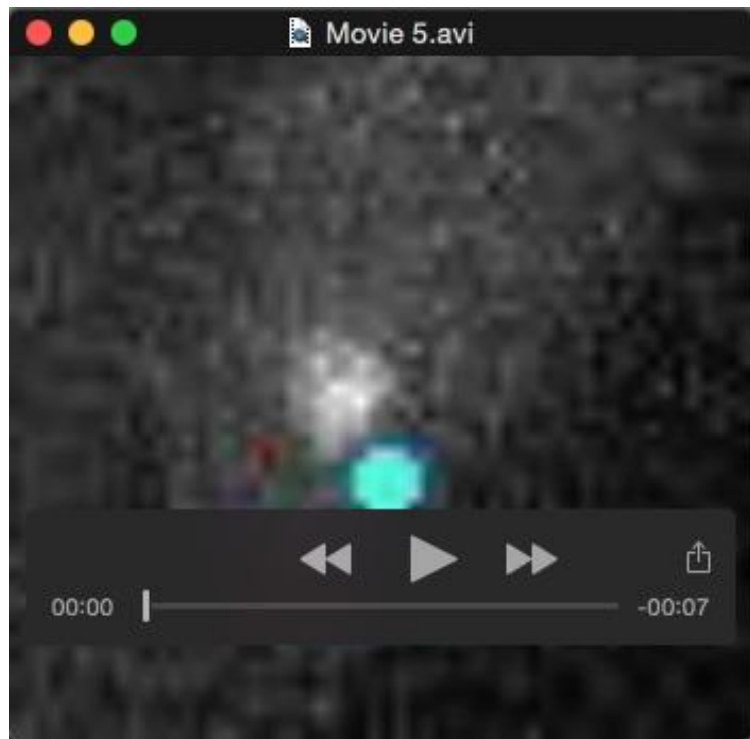
Movie S3. Representative of PIV analysis of *MZdchs1b^{fh275/fh275}* embryo.

Time-lapse imaging of *MZdchs1b^{fh275/fh275}* embryo beginning at 8 mpf with interval of 1 minute for 45 minutes. PIV analysis overlay bright field imaging. Red->animal pole ward. Blue->vegetal pole ward.



Movie S4. Cell division in MZdchs1b^{flh275/flh275}embryo.

Time-lapse imaging of MZdchs1b^{flh275/flh275}, Tg[β-actin:Utrophin-GFP] embryo beginning at 8 cells with interval of 2 minute for 31 minutes. Lineage trace indicated by color of dots. Abnormal cell divisions indicated with outlining.



Movie S5. Single abnormal cell division in *MZdchs1b^{flh275/flh275}* embryo.

Time-lapse imaging of *MZdchs1b^{flh275/flh275}* embryo injected with H2B-GFP beginning at 32 cells with interval of 1 minute for 22 minutes. Lineage trace indicated by color of dots.